

Interplay of topology and interactions in quantum Hall topological insulators: U(1) symmetry, tunable Luttinger liquid, and interaction-induced phase transitions

Maxim Kharitonov, Stefan Juergens, and Björn Trauzettel
*Institute for Theoretical Physics and Astrophysics,
 University of Würzburg, 97074 Würzburg, Germany*

We consider a class of *quantum Hall topological insulators*: topologically nontrivial states with zero Chern number at finite magnetic field, in which the counter-propagating edge states are protected by a symmetry (spatial or spin) other than time-reversal. HgTe-type heterostructures and graphene are among the relevant systems. We study the effect of electron interactions on the topological properties of the system. We particularly focus on the vicinity of the topological phase transition, marked by the crossing of two Landau levels, where the system is a strongly interacting quantum Hall ferromagnet. We analyse the edge properties using the formalism of the nonlinear σ -model. We establish the symmetry requirement for the topological protection in this interacting system: effective continuous U(1) symmetry with respect to uniaxial isospin rotations must be preserved. If U(1) symmetry is preserved, the topologically nontrivial phase persists; its edge is a helical Luttinger liquid with highly tunable effective interactions. We obtain explicit analytical expressions for the parameters of the Luttinger liquid. However, U(1) symmetry may be broken, either spontaneously or by U(1)-asymmetric interactions. In either case, interaction-induced transitions occur to the respective topologically trivial phases with gapped edge charge excitations.

I. INTRODUCTION

Interacting topological^{1–9} systems are currently an active area of research^{10–17}. Of particular interest are the situations, when interactions can change the single-particle picture in a qualitative way and lead to effects not present in the non-interacting system. Theoretical proposals of such a nontrivial behavior include a “topological Mott insulator”¹⁰, “Kondo topological insulator”^{11,12}, interaction-induced topological phases in graphene^{13,14}, and first-order topological phase transitions¹⁵.

Most of these predictions require sufficiently strong electron interactions and were made for “strongly cor-

related” materials. Meanwhile, most of the materials to date that have been experimentally firmly established as topological insulators, such as HgTe/CdTe³, BiSb⁴, or BiSe⁵ compounds, are rather weakly interacting due to efficient screening of the Coulomb interactions.

It is thus desirable to expand the range of possibilities to attain the regime of strong effective interactions in topological systems, and it is even more desirable to be able to tune the strength of interactions by experimentally feasible means.

In this work, we have identified a class of topological systems, in which such conditions can be realized even for weak bare interactions by applying the orbital magnetic field. The interactions are tunable by the magnetic field and their strength is controlled by the proximity to the topological phase transition. The vicinity of the topological phase transition is automatically the regime of strong effective interactions, in which Coulomb interactions are crucial for both bulk and edge properties and lead to a nontrivial interplay of topological and interacting phenomena.

An important theoretical advantage of such a system is that it can be analyzed in a well-controlled way. In particular, this allowed us to determine the symmetry requirements for topological protection in this system, which is one of the key questions raised in the studies of interacting topological systems.

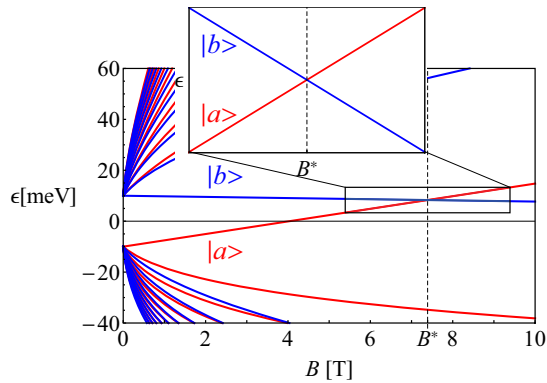


FIG. 1: (Color online) One possible type of the Landau level (LL) structure of a quantum Hall topological insulator (QHTI). At the single-particle topological phase transition point, LLs of different symmetries, labeled a (red) and b (blue), cross. The spectrum shown was calculated for the Bernevig-Hughes-Zhang model^{2,18} with a perpendicular orientation of the magnetic field; in this case, LLs a are distinguished by the spatial inversion parity, even and odd.

A. Quantum Hall topological insulators

We consider a class of electron systems that we dub *quantum Hall topological insulators* (QHTIs): (quasi) two-dimensional (2D) electron systems with zero Chern number $\nu = 0$ at finite magnetic field B that can still be topologically non-trivial (TnT) and exhibit counter-propagating edge states. Since the time-reversal sym-

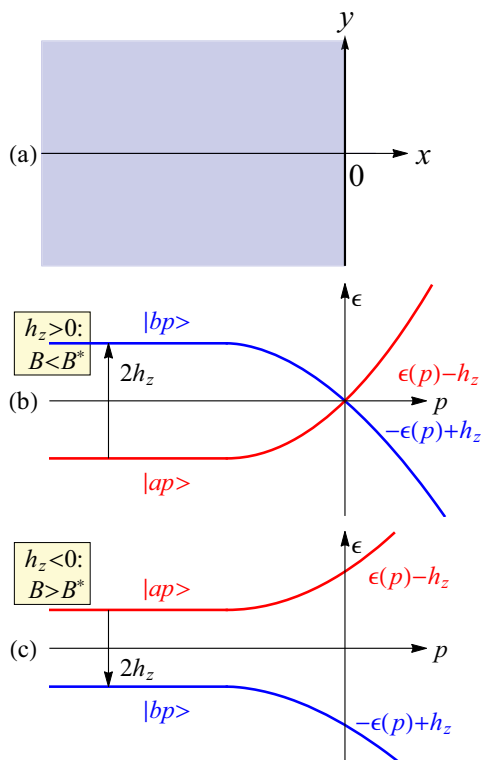


FIG. 2: (Color online) (a) Half-infinite sample occupying the region $x \leq 0$. (b) and (c) Schematics of the edge spectrum of a QHTI in the Landau gauge, including only the two intersecting LLs a and b of interest, see Fig. 1. The single-particle states are labeled by the conserved 1D momentum p in the y direction. The states located in the bulk and at the edge correspond to the values $p \lesssim 0$ and $p \gtrsim 0$, respectively. In the topologically non-trivial (TnT) phase at lower fields $B < B^*$ (b), the edge states cross and are gapless. In the topologically trivial (TT) phase at higher fields $B^* < B$ (c), the edge states do not cross and are gapped.

metry is broken by the magnetic field, the TnT phase must be protected by some other symmetry. In a system with appreciable spin-orbit interaction, such symmetry is some spatial symmetry (e.g., inversion, reflection, or rotation). In a system with negligible spin-orbit interaction, axial spin rotation symmetry can also play the role of such symmetry. We will refer to this symmetry responsible for the topological protection of a *noninteracting* QHTI as the *physical symmetry*, in order to contrast it to the *effective*, or *emergent*, $U(1)$ symmetry, which will be demonstrated to be central for an *interacting* system.

One possible type of the Landau level (LL) structure of a QHTI would exhibit a crossing of two LLs at some value B^* of the magnetic field: one LL, to be labelled a , originates from the valence band and moves upward with increasing B , and the other LL, to be labelled b , originates from the conduction band and moves downward, see Fig. 1. This crossing is a point of the topological phase transition of a QHTI, separating the TnT phase with counter-propagating states at lower $B < B^*$, and

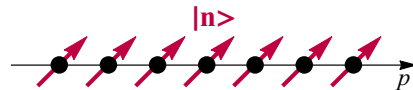


FIG. 3: (Color online) Quantum Hall ferromagnet (QHF) state realized at the crossing of LLs at half-filling. For each momentum p , one electron occupies the state $|n\rangle$ with given isospin \mathbf{n} , see Eqs. (1.1), (1.2), and (1.3) and Fig. 4.

the topologically trivial (TT) phase with gapped edge states at higher $B > B^*$, see Fig. 2. Other variants of the LL structure in QHTIs are also possible.

A number of previously studied theoretical models and real physical systems are relevant to the class of QHTIs. The single-particle behavior of Figs. 1 and 2 has been identified¹⁸ in the Bernevig-Hughes-Zhang model² for the direction of the magnetic field perpendicular to the 2D structure. This behavior is likely to have topological origin and be protected a spatial symmetry. This model is directly relevant to HgTe/CdTe³ and InAs/GaSb^{6,7} heterostructures, which are established 2D topological insulators at zero field, protected by the time-reversal symmetry.

Other likely QHTI systems are graphene single- and multi-layer structures. Noninteracting graphene exhibits counter-propagating edge states¹⁹ at finite magnetic field due to spin splitting by the Zeeman field and the fact that graphene is a semimetal. It can be seen as a QHTI protected by the continuous axial spin rotation symmetry²⁰. Although directly relevant, graphene also has a few peculiarities and its LL structure differs from that in Fig. 1; the focus of the present work are the QHTIs with a spectrum of the type in Fig. 1.

To be clear, we emphasize that according to the above definition QHTIs are not necessarily new topological systems symmetry-wise, in regard to the existing classifications^{21–24}. The key requirement here is that the orbital magnetic field is explicitly present and the system is in the quantum Hall (QH) regime. This leads to physical phenomena, stemming mainly from the “flat-band” property of the LL spectrum in the bulk (Fig. 2), that are specific to the QH regime and otherwise may hardly be realized.

B. Quantum Hall ferromagnet at the topological phase transition

The QHTIs with the LL structure as in Fig. 1 are particularly appealing for the study of the interplay of interactions and topology: due to the near degeneracy of the two LLs in vicinity of the single-particle topological phase transition point B^* , electron interactions become the dominant effect that drives the physics there. Thus, in QHTIs, effective interactions are tunable by the magnetic field, and the regime of strong effective interactions

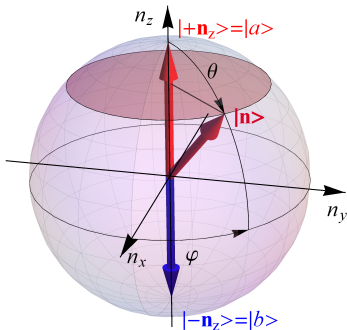


FIG. 4: (Color online) Bloch sphere of the isospin \mathbf{n} in the 2D space of a and b LLs [Eqs. (1.1), (1.2), and (1.3)]. The north $|+\mathbf{n}_z\rangle = |a\rangle$ and south $|-\mathbf{n}_z\rangle = |b\rangle$ poles corresponds to the occupation of the a and b LLs, respectively. Any other state is a coherent mixture of the $|a\rangle$ and $|b\rangle$ states.

is experimentally accessible even in a system with weak bare interactions.

In this work, we investigate the effect of electron interactions on the topological properties of QHTIs with the LL structure shown in Fig. 1, particularly focusing on the regime of strong effective interactions in the vicinity of the single-particle topological phase transition.

The zero Chern number $\nu = 0$ corresponds to half-filling of the two crossing LLs a and b , with on average one electron per two states. Analogous to the Hund exchange mechanism in atoms, at such commensurate filling factor, interactions make the electron system particularly prone to polarization in the 2D ab space. This results in the formation of the “ferromagnetic” ground state, see Fig. 3, in which electrons at each orbital occupy exactly the same state

$$|\mathbf{n}\rangle = \chi_a(\mathbf{n})|a\rangle + \chi_b(\mathbf{n})|b\rangle, \quad (1.1)$$

$$\chi(\mathbf{n}) = \begin{pmatrix} \chi_a(\mathbf{n}) \\ \chi_b(\mathbf{n}) \end{pmatrix} = \begin{pmatrix} e^{-\frac{1}{2}\varphi} \cos \frac{\theta}{2} \\ e^{\frac{1}{2}\varphi} \sin \frac{\theta}{2} \end{pmatrix}, \quad (1.2)$$

characterized by the unit-vector “isospin”

$$\mathbf{n} = (n_x, n_y, n_z) = (\sin \theta \cos \varphi, \sin \theta \sin \varphi, \cos \theta), \quad \mathbf{n}^2 = 1, \quad (1.3)$$

$$|\mathbf{n}\rangle\langle\mathbf{n}| = \frac{1}{2}(\tau_0 + \boldsymbol{\tau} \cdot \mathbf{n}), \quad (1.4)$$

see Fig. 4. Throughout, τ_0 and $\boldsymbol{\tau} = (\tau_x, \tau_y, \tau_z)$ will denote the unity and Pauli matrices in the ab space.

Exactly at the crossing point and in the approximation of the SU(2)-symmetric interactions in the ab space, the isospin \mathbf{n} can be completely arbitrary and the state describes spontaneous breaking of SU(2) symmetry. This phenomenon is referred to as *quantum Hall ferromagnetism* (QHFMism)²⁵.

The bulk single-particle and interaction effects responsible for the deviation from this fully degenerate SU(2)-symmetric situation, as well the effect of the edge, can be taken into account within a low-energy field theory, the nonlinear σ -model, for the isospin order parameter (OP) $\mathbf{n}(\mathbf{r}; t)$ generalized to configurations slowly varying in time and space. We derive the closed form of such σ -model in the coordinate space. Crucial for the description of the edge properties, we incorporate the effect of the edge as a boundary condition for the order parameter. This allows us to study most properties of interest analytically. The analysis of the properties of the edge excitations follows the approach developed in Refs. 26–30 for the $\nu = 0$ QH state in graphene. Their properties are governed by the spatially inhomogeneous textures of the order parameter at the edge.

We calculate the bulk phase diagram, ground state edge textures, and edge charge excitations. For the interacting TnT phase, we derive and analyze the low-energy theory for the gapless edge excitations.

C. Main findings

As the central general result, we find that topological properties of this interacting many-body system are directly tied to its effective symmetry: the U(1) symmetry with respect to rotations about the isospin z axis is responsible for the topological protection.

We demonstrate that if U(1) symmetry is preserved, the single-particle TnT phase with fully filled $|a\rangle$ LL, corresponding to $\mathbf{n} = \mathbf{n}_z = (0, 0, 1)$ isospin in the QHFM formalism, remains TnT in the presence of interactions in most of the range $0 \leq B < B^*$. The edge excitations remain gapless but take the form of collective excitations described by the helical Luttinger liquid. We obtain explicit analytical expressions for the parameters of the Luttinger liquid in the QHFM regime. We find that the effective interactions in this Luttinger liquid are highly tunable: weak (with the interaction parameter³¹ $\mathcal{K} \approx 1$) at small magnetic fields $B \ll B^*$, but strong ($\mathcal{K} \ll 1$) in the QHFM regime in the vicinity of the single-particle phase transition B^* .

More precisely, “preserved U(1) symmetry” means that *both* the bulk ground state and the many-body Hamiltonian are U(1)-symmetric. According to the violation of one of these conditions, we identify two mechanisms of the U(1) symmetry breaking, which lead to the loss of topological protection and eventual transitions to the TT phases.

First, U(1) could be broken spontaneously: upon increasing B , a second-order phase transition from the TnT phase $\mathbf{n} = \mathbf{n}_z$ to the phase with spontaneously broken U(1) symmetry may occur. The gap in the edge excitation spectrum of this broken-U(1)-symmetry phase grows monotonically upon further increasing B , starting from the zero value at the phase transition. Also, upon approaching this phase transition from the TnT

$\mathbf{n} = \mathbf{n}_z$ phase, the edge Luttinger liquid becomes infinitely strongly interacting ($\mathcal{K} \rightarrow 0$).

Second, the many-body Hamiltonian can be U(1)-asymmetric: *interaction terms* can be present that fully respect the physical symmetry, responsible for the topological protection of the non-interacting system, but break U(1) symmetry. Such terms transform the Luttinger liquid model for the edge excitations of the TnT $\mathbf{n} = \mathbf{n}_z$ phase into the sine-Gordon model³¹. As B is increased, such terms will result in the phase transition to the state with broken U(1) symmetry at the edge and gapped edge excitations.

In either of the scenarios, the phase transitions from the TnT to the TT phases occur at the magnetic fields B lower than the single-particle phase transition point B^* and are thus *interaction-induced topological* quantum phase transitions.

The rest of the paper is organized as follows. In Sec. II, we present the projected Hamiltonian. In Sec. III, we derive the low-energy theory for the QHFM. In Sec. IV, we obtain the bulk phase diagram. In Sec. V, we obtain the ground state configurations for a system with an edge. In Sec. VI, we study the edge charge excitations. In Sec. VII, we derive the Luttinger liquid model for the edge excitations in the TnT phase. In Sec. VIII, we establish U(1) symmetry as the requirement for topological protection. In Sec. IX, we present concluding remarks.

II. PROJECTED HAMILTONIAN

A. Restricted Hilbert space of two intersecting Landau levels

We will work under the approximation where only the two intersecting LLs a and b in Fig. 1 are taken into account, while other LLs are neglected. This is a standard approximation for quantum Hall systems, justified for weak Coulomb interactions, when the energy separation between the LLs of interest and other LLs is much larger than the interaction energy scale set by the Coulomb energy

$$\frac{e_*^2}{l_{B_z}} = \frac{e^2}{\varkappa l_{B_z}}. \quad (2.1)$$

Here, e_* is the electron charge screened by the dielectric environment with the constant \varkappa , and

$$l_{B_z} = \sqrt{\frac{c}{eB_z}}$$

is the magnetic length, in which e is the electron charge, c is the speed of light, and B_z is the component of the magnetic field perpendicular to the sample plane, $B^2 = B_z^2 + B_\perp^2$. We assume arbitrary orientation of the magnetic field relative to the quasi 2D sample, although this point will not be important.

We will work in the Landau gauge, in which the single-particle states are characterized by the one-dimensional momentum p along the edge y direction. The single-particle states of the LLs of interest are

$$|ap\rangle \text{ and } |bp\rangle. \quad (2.2)$$

We assume no discrete degeneracies (such as valleys) of these LLs.

We consider a half-infinite two-dimensional sample occupying the region $x < 0$, see Fig. 2. The states with $p \lesssim 0$ are then the bulk states, for which the coordinate-momentum correspondence holds, and the states with $p \gtrsim 0$ correspond to the edge states, localized over l near the edge. The electron annihilation operators will be denoted as c_{ap} and c_{bp} ; in the formulas below, we join them into a two-component spinor

$$\hat{c}_p = \begin{pmatrix} c_{ap} \\ c_{bp} \end{pmatrix} \quad (2.3)$$

for compactness.

B. U(1)-symmetric projected Hamiltonian

We first consider the following many-body “projected” Hamiltonian, operating within the states (2.2) of the intersecting LLs:

$$\hat{H} = \hat{H}_{1\circ} + \hat{H}_{1\circ}^{\text{edge}} + \hat{H}_{2\odot} + \hat{H}_{2\circ}, \quad (2.4)$$

$$\hat{H}_{1\circ} = -h_z \sum_p \hat{c}_p^\dagger \tau_z \hat{c}_p, \quad (2.5)$$

$$\hat{H}_{1\circ}^{\text{edge}} = \sum_p \epsilon(p) \hat{c}_p^\dagger \tau_z \hat{c}_p, \quad (2.6)$$

$$\hat{H}_{2\odot} = \frac{1}{2} \sum_{p_1+p_2=p'_1+p'_2} V(0|_{p_2 p'_2}^{p_1 p'_1}) : [\hat{c}_{p_1}^\dagger \hat{c}_{p'_1}] [\hat{c}_{p_2}^\dagger \hat{c}_{p'_2}] :, \quad (2.7)$$

$$\hat{H}_{2\circ} = \frac{1}{2} \sum_{p_1+p_2=p'_1+p'_2} \sum_{\alpha=x,y,z} V(\alpha|_{p_2 p'_2}^{p_1 p'_1}) : [\hat{c}_{p_1}^\dagger \tau_\alpha \hat{c}_{p'_1}] [\hat{c}_{p_2}^\dagger \tau_\alpha \hat{c}_{p'_2}] :, \quad V(x|_{p_2 p'_2}^{p_1 p'_1}) = V(y|_{p_2 p'_2}^{p_1 p'_1}). \quad (2.8)$$

The labels 1 and 2 designate single-particle and two-particle interaction terms, respectively; the labels \circ and \odot are explained below.

The term (2.5) describes the energy spacing between the two LLs of interest, equal to $2h_z$. The energy $h_z(B)$ is a function of the magnetic field B (Figs. 1 and 2): it decreases monotonically with increasing the magnetic field, starting from positive values and changing to negative values at the crossing point $B = B^*$. Close to the crossing point, one may expand it to the linear order as

$$h_z(B) \approx -|\partial_B h_z(B^*)|(B - B^*). \quad (2.9)$$

Next, the term (2.6) describes the effect of the edge. The dispersion function $\epsilon(p) > 0$ is shown schematically in Fig. 2; it has a plateau $\epsilon(p) \approx 0$ in the bulk ($p \lesssim 0$) and grows monotonically at the edge $p \gtrsim 0$. Note that although the two branches at the edge do not have to be exactly particle-hole symmetric and an additional energy term $\epsilon_0(p)\tau_0$ could be added, it produces only a trivial \mathbf{n} -independent term in the σ -model derived below; so, we neglect it.

Crucially, due to the assumed topological protection by the physical symmetry, the single-particle terms $\hat{H}_{1\circ} + \hat{H}_{1\circ}^{\text{edge}}$ do not couple the $|ap\rangle$ and $|bp\rangle$ states. The single-particle spectrum $\pm[-h_z + \epsilon(p)]$ of $\hat{H}_{1\circ} + \hat{H}_{1\circ}^{\text{edge}}$ describes two LL with counter-propagating edge states at $0 < h_z$ (TnT phase) and a fully gapped spectrum, both in the bulk and at the edge, at $h_z < 0$ (TT phase).

Due to this decoupling of the $|ap\rangle$ and $|bp\rangle$ states, the single-particle Hamiltonian $\hat{H}_{1\circ} + \hat{H}_{1\circ}^{\text{edge}}$ [Eqs. (2.5) and (2.6)] possesses U(1) symmetry with respect to continuous rotations about the isospin z axis, as described by the matrix

$$\hat{D}(\phi) = \begin{pmatrix} e^{-i\frac{\phi}{2}} & 0 \\ 0 & e^{i\frac{\phi}{2}} \end{pmatrix} \quad (2.10)$$

acting on the spinor (1.2) in the ab space as

$$\hat{D}(\phi)\chi(\theta, \varphi) = \chi(\theta, \varphi + \phi). \quad (2.11)$$

Here, θ and φ are the angles of the spherical parametrization of the isospin [Eqs. (1.2) and (1.3)]

As we shall find below, this effective continuous U(1) symmetry is central to the properties of the edge charge excitations of the interacting system and the associated topological properties. For this reason, we consider the form of two-particle interactions, presented in Eqs. (2.7) and (2.8), that preserves this U(1) symmetry. We also split these interactions into two parts, the SU(2)-symmetric part $\hat{H}_{2\odot}$ [Eq. (2.7)] and the SU(2)-asymmetric U(1)-symmetric part $\hat{H}_{2\circ}$ [Eq. (2.8)] (The terms with the structure $\hat{1} \otimes \tau_z$ are also U(1)-symmetric, but in the σ -model below they lead to an inconsequential shift of the position of single-particle transition point; therefore, we discard them in order not to overburden the expressions.). The exact form of the matrix elements $V(\alpha|_{p_2 p'_2}^{p_1 p'_1})$, $\alpha = 0, x, y, z$, will not matter for our considerations, only the presented structure of the terms in the isospin space will. The only condition we assume is that the U(1)-asymmetric terms are much smaller than the SU(2)-symmetric ones, in order to make the low-energy field theory a controlled expansion. The SU(2)-symmetric interactions have the typical scale of the Coulomb energy,

$$\sum_{p_2} V(0|_{p_2 p_1}^{p_1 p_2}) \sim \frac{e_*^2}{l_{Bz}}. \quad (2.12)$$

The Hamiltonian \hat{H} [Eq. (2.4)] thus possesses U(1) symmetry. We now consider possible U(1)-asymmetric terms.

C. U(1)-asymmetric terms

The mechanisms of (non-spontaneous) U(1) symmetry breaking could be grouped into two categories according to an important symmetry distinction between them.

1) One category is when already the physical symmetry responsible for the topological protection of a noninteracting system is violated. Consequently, the U(1) symmetry is then broken already at the single-particle level. The corresponding terms have the form of the isospin

“Zeeman” field acting in the xy plane:

$$\hat{H}_{1\emptyset} = -h_{\perp} \sum_p \hat{c}_p^{\dagger} (\tau_x \cos \varphi_{1\emptyset} + \tau_y \sin \varphi_{1\emptyset}) \hat{c}_p. \quad (2.13)$$

Such terms result in the coupling between the a and b LLs. The “orientation” of this field in the xy plane, set by the angle $\varphi_{1\emptyset}$, depends on the choice of the relative phase factor between the $|ap\rangle$ and $|bp\rangle$ states and is largely arbitrary.

2) Another category is when the physical symmetry is preserved. Then no single-particle terms breaking U(1) symmetry are allowed. However, interactions that preserve the physical symmetry but break U(1) symmetry could be present:

$$\hat{H}_{2\emptyset} = \frac{1}{2} \sum_{\substack{p_1+p_2 \\ =p'_1+p'_2}} \sum_{\alpha_1 \alpha_2}^{\emptyset} V_{(\alpha_2 | p_2 p'_2)}^{(\alpha_1 | p_1 p'_1)} : [\hat{c}_{p_1}^{\dagger} \tau_{\alpha_1} \hat{c}_{p'_1}] [\hat{c}_{p_2}^{\dagger} \tau_{\alpha_2} \hat{c}_{p'_2}] : \quad (2.14)$$

where the sum $\sum_{\alpha_1 \alpha_2}^{\emptyset}$ contains only U(1)-asymmetric terms. The structure of such interactions depends on specific physical symmetry, which does provide some constraints on the matrix elements $V_{(\alpha_2 | p_2 p'_2)}^{(\alpha_1 | p_1 p'_1)}$, but for most physical symmetries such U(1)-asymmetric interactions would be allowed. For the σ -model approach we employ, however, the detailed knowledge of their structure is not necessary, only the corresponding anisotropy function is required. The latter can be derived using symmetry considerations, as we illustrate in Sec. III C.

III. LOW-ENERGY NONLINEAR σ -MODEL

A. Quantum Hall “ferromagnet”

Close to the crossing point $h_z = 0$ of the LLs, the SU(2)-symmetric part $\hat{H}_{2\odot}$ [Eq. (2.7)] of the electron interactions is the dominant term in the Hamiltonian \hat{H} [Eq. (2.4)]: its typical scale e_*^2/l_{B_z} [Eq. (2.12)] exceeds the energies of all other terms. It is straightforward to show that, at half-filling of the two LLs $|ap\rangle$ and $|bp\rangle$, the Slater determinant state

$$\Psi(\mathbf{n}) = \prod_{\text{bulk } p} c_{\mathbf{n}p}^{\dagger} |0\rangle \quad (3.1)$$

is an exact eigenstate of $\hat{H}_{2\odot}$. Here, $|0\rangle$ is the “vacuum” state with both LLs empty and

$$c_{\mathbf{n}p}^{\dagger} = \chi_a(\mathbf{n}) c_{ap}^{\dagger} + \chi_b(\mathbf{n}) c_{bp}^{\dagger} \quad (3.2)$$

is the operator creating an electron in the state $|\mathbf{n}\rangle$ [Eq. (1.1)] with the isospin \mathbf{n} [Eq. (1.3)]. The isospin can be visualized by means of the Bloch sphere, see Fig. 4. According to Eq. (1.1), the isospin at the “poles” of the Bloch sphere $\mathbf{n} = \pm \mathbf{n}_z$ ($\theta = 0, \pi$), corresponds to pure $|\mathbf{n}_z\rangle = |a\rangle$ or $|\mathbf{n}_z\rangle = |b\rangle$ states. Any other state with

$-1 < n_z < 1$ ($0 < \theta < \pi$) is a coherent mixture of $|a\rangle$ and $|b\rangle$ states.

For a wide class of repulsive interactions, one can expect this eigenstate to be an exact ground state by the Hund’s rule argument. This is the main assumption of the QHFMism theory²⁵, also employed in this paper.

Importantly, the many-body wave-function $\Psi(\mathbf{n})$ is an eigenstate of $\hat{H}_{2\odot}$ for any choice of the isospin \mathbf{n} . It thus describes the state with spontaneously broken SU(2) symmetry; the unit vector \mathbf{n} represents the OP of the family of degenerate ground states.

B. U(1)-symmetric nonlinear σ -model

The effects of the other, SU(2)-asymmetric, terms in the Hamiltonian on the ground state and excitations of the QHFM can be taken into account within a low-energy field theory, the σ -model. As long as the energy scales of these terms are much smaller than the Coulomb scale (2.12) of the SU(2)-symmetric interactions, the σ -model presents a controlled systematic low-energy expansion about the exact ground state (3.1) of $\hat{H}_{2\odot}$.

For the Hamiltonian given by Eqs. (2.4), (2.13), and (2.14), the derivation of the σ -model is rather standard and follows the general recipe²⁵. The new aspect is incorporating the effect of the edge with counter-propagating states into the real-space σ -model, which we perform below at the end of this section.

In the nonlinear σ -model, the homogeneous and static isospin OP \mathbf{n} of the state (3.1) is generalized to configurations $\mathbf{n}(\mathbf{r}; t)$ that vary slowly in time and space. The constraint

$$\mathbf{n}^2(\mathbf{r}; t) = 1$$

is satisfied locally.

The low-energy dynamics and energetics is described by the Lagrangian functional; for the bulk part (all terms except $\hat{H}_{1\odot}^{\text{edge}}$) of the U(1)-symmetric Hamiltonian (2.4), it has the form

$$\mathbb{L}[\mathbf{n}] = \mathbb{K}[\mathbf{n}] - \mathbb{E}[\mathbf{n}] = \int \frac{d^2\mathbf{r}}{s} L[\mathbf{n}], \quad L[\mathbf{n}] = K[\mathbf{n}] - E[\mathbf{n}] \quad (3.3)$$

$$\mathbb{K}[\mathbf{n}] = \int \frac{d^2\mathbf{r}}{s} K[\mathbf{n}], \quad K[\mathbf{n}] = \frac{\dot{\varphi}}{2} \cos \theta, \quad (3.4)$$

$$\mathbb{E}[\mathbf{n}] = \int \frac{d^2\mathbf{r}}{s} E[\mathbf{n}], \quad E[\mathbf{n}] = \frac{\rho}{2} (\nabla \mathbf{n})^2 + \mathcal{E}(n_z), \quad (3.5)$$

$$\mathcal{E}(n_z) = \frac{u}{2} n_z^2 - h_z n_z = \frac{u}{2} \cos^2 \theta - h_z \cos \theta. \quad (3.6)$$

The Lagrangian $\mathbb{L}[\mathbf{n}]$ is given by the difference of the kinetic $\mathbb{K}[\mathbf{n}]$ and energy $\mathbb{E}[\mathbf{n}]$ terms. The spatial integration $\int d^2\mathbf{r} \dots$ is performed over the region $x < 0$ occupied by the half-infinite sample. We introduce the normalization factor

$$s = 2\pi l_{B_z}^2$$

equal to the area threaded by one magnetic flux quantum; $1/s$ is also the electron density per one LL. This way, the respective densities $L[\mathbf{n}]$, $K[\mathbf{n}]$, $E[\mathbf{n}]$ are defined per this area s and have the dimension of energy.

The kinetic term $\mathbb{K}[\mathbf{n}]$ [Eq. (3.4)] contains the time derivative and can be presented explicitly in terms of the spherical angles θ and φ parameterizing the isospin [Eq. (1.3)]. Note that the form of $K[\mathbf{n}]$ is not unique, but is defined up to a full time derivative, which results in an inconsequential constant contribution to the action $\int dt \mathbb{L}[\mathbf{n}]$.

The energy functional $\mathbb{E}[\mathbf{n}]$ [Eq. (3.5)] consists of the gradient term $\frac{\rho}{2}(\nabla\mathbf{n})^2$ and the energy function $\mathcal{E}(n_z)$ [Eq. (3.6)]. The gradient term describes the energy cost of a spatially inhomogeneous configuration; to the leading order, the stiffness

$$\rho = \frac{l_{B_z}^4}{4} \sum_{p_2} V_{p_2}^{(0|p_1 p_2)} (p_1 - p_2)^2$$

is expressed in terms of the SU(2)-symmetric $\hat{H}_{2\circ}$ interactions.

The energy function $\mathcal{E}(n_z)$ describes the effect of the bulk terms $\hat{H}_{1\circ} + \hat{H}_{2\circ}$ that have the symmetry lower than SU(2). To derive it, it is sufficient to take the expectation value

$$\mathcal{E}(n_z) = \frac{1}{\mathcal{N}} \langle \Psi(\mathbf{n}) | \hat{H}_{1\circ} + \hat{H}_{2\circ} | \Psi(\mathbf{n}) \rangle \quad (3.7)$$

of the corresponding terms with respect to the state $\Psi(\mathbf{n})$ [Eq. (3.1)] ($\mathcal{N} = \sum_p 1 = \int \frac{d^2\mathbf{r}}{s} 1$ is the number of orbital states, equal to the number of flux quanta threading the sample.) The term $\frac{\rho}{2} n_z^2$ quadratic in \mathbf{n} arises from the SU(2)-asymmetric two-particle interactions $\hat{H}_{2\circ}$ and can be referred to as the ‘‘anisotropy’’ term; the anisotropy energy equals

$$\begin{aligned} u &= u_z - u_{\perp}, \quad u_{\perp} \equiv u_x = u_y, \\ u_{\alpha} &= \sum_{p_2} [V_{p_2}^{(\alpha|p_1 p_2)} - V_{p_2}^{(\alpha|p_2 p_1)}], \quad \alpha = x, y, z. \end{aligned}$$

We will consider the more interesting case of positive anisotropy energy

$$u > 0,$$

which is called ‘‘easy-plane’’ anisotropy, since the energy $\frac{\rho}{2} n_z^2$ alone is minimized by the isospin in the plane $n_z = 0$.

The only remaining term in the U(1)-symmetric Hamiltonian \hat{H} [Eq. (2.4)] that needs to be taken into account is $\hat{H}_{1\circ}^{\text{edge}}$, which describes the edge. Its effect can be presented as an effective boundary condition for the order parameter $\mathbf{n}(\mathbf{r}; t)$ as follows. We first note that the edge states ($p \gtrsim 0$) are also ‘‘half-filled’’ (one electron per two states) and thus their occupation can be described by the same isospin OP: the filling factor remains the same for both bulk ($p \lesssim 0$) and edge ($p \gtrsim 0$) states. At such p

that the energy $\epsilon(p)$ becomes much greater than the energies u and h_z of the SU(2)-asymmetric terms, electrons occupy the ‘‘hole’’ branch of the edge spectrum, i.e., the states $|bp\rangle$ with the negative energy $-\epsilon(p)$, which corresponds to $\mathbf{n} = -\mathbf{n}_z$. Since the edge states with $p \gtrsim 0$ are localized at spatial scales $\sim l_{B_z}$ near the edge $x = 0$ of the sample and $\mathbf{n}(\mathbf{r}; t)$, by assumption, varies at much larger scales, the effect of the edge may be described in the real space by the boundary condition

$$\mathbf{n}(x = 0, y; t) = -\mathbf{n}_z, \quad \mathbf{n}_z = (0, 0, 1). \quad (3.8)$$

Thus, the effect of the edge amounts to ‘‘pinning’’ the OP in the state that corresponds to the occupation of the ‘‘hole’’ branch of the edge spectrum.

Equations (3.3)-(3.6) for the Lagrangian and Eq. (3.8) for the boundary condition constitute the closed-form low-energy σ -model in the coordinate space for the considered QHFM system with an edge, originating from the Hamiltonian \hat{H} [Eq. (2.4)]. Naturally, the model inherits the U(1) symmetry [Eqs. (2.10) and (2.11)] of the Hamiltonian (2.4) and is invariant under the rotations of the isospin about the z axis:

$$\varphi(\mathbf{r}; t) \rightarrow \varphi(\mathbf{r}; t) + \phi.$$

The additional terms in the σ -model originating from the U(1)-asymmetric terms (2.13) and (2.14) in the full Hamiltonian, Sec. II C, are considered below.

C. U(1)-asymmetric terms

The single-particle term $\hat{H}_{1\circ}$ [Eq. (2.13)] that breaks U(1) symmetry produces the following additional contribution to the energy function (3.6):

$$\begin{aligned} \mathcal{E}_{1\circ}(\mathbf{n}) &= \frac{1}{\mathcal{N}} \langle \Psi(\mathbf{n}) | \hat{H}_{1\circ} | \Psi(\mathbf{n}) \rangle \\ &= -h_{\perp} (n_x \cos \varphi_{1\circ} + n_y \sin \varphi_{1\circ}) \\ &= -h_{\perp} \sin \theta \cos(\varphi - \varphi_{1\circ}). \end{aligned} \quad (3.9)$$

The structure of the anisotropy energy function arising from the U(1)-asymmetric two-particle interactions $\hat{H}_{2\circ}$ [Eq. (2.14)] depends on the specific physical symmetry. It can be derived via group-theoretical considerations without using any information about the interaction matrix elements in Eq. (2.14). As an example, we will consider the inversion symmetry.

In this case, the LLs states a and b are characterized by opposite inversion parities $+$ and $-$. Therefore, the isospin components transforming according to Eq. (1.4) as $n_{x,y} \sim |a\rangle\langle b|$ and $n_z \sim |a\rangle\langle a| - |b\rangle\langle b|$ have $-$ and $+$ parities, respectively.

The anisotropy function arising from two-particle interactions is a quadratic function of \mathbf{n} . It must be invariant under inversion, i.e., have $+$ parity. All quadratic functions with $+$ parity are

$$\{n_z^2, n_x^2, 2n_x n_y, n_y^2\}.$$

The most general form of the anisotropy function is an arbitrary linear combination of these terms.

It is convenient to choose the basis functions as

$$\{n_x^2 + n_y^2 + n_z^2, n_z^2 - n_x^2 - n_y^2, n_x^2 - n_y^2, 2n_x n_y\}.$$

Then, the combination $n_x^2 + n_y^2 + n_z^2 = 1$ preserves SU(2) symmetry and, due to the constraint (1.3), is \mathbf{n} -independent; the combination $n_z^2 - n_x^2 - n_y^2 = 2n_z^2 - 1$ preserves U(1) symmetry and depends only on n_z . These two functions produce, up to a constant, the U(1)-symmetric anisotropy function $\frac{1}{2}un_z^2$ in $\mathcal{E}(n_z)$ [Eq. (3.6)]. An arbitrary linear combination

$$\begin{aligned} \mathcal{E}_{2\varnothing}(\mathbf{n}) &= \frac{1}{2}[u_+(n_x^2 - n_y^2) + u_\times 2n_x n_y] \\ &= \frac{1}{2}u_{2\varnothing} \sin^2 \theta \cos 2(\varphi - \varphi_{2\varnothing}) \end{aligned} \quad (3.10)$$

of the two remaining functions represents the U(1)-asymmetric contribution to the anisotropy function.

D. Outline of the approach

The remaining part of the paper is devoted to the analysis of the obtained σ -model, with the focus on the properties of the edge excitations. The fact that the effect of the edge has been reduced to the boundary condition (3.8) in the coordinate space is a technical advantage that will facilitate the analysis of the problem and enable us to obtain explicit analytical expressions for many quantities of interest.

The approach we use to study the edge excitations follows that developed in a series of papers²⁶⁻³⁰ for the ferromagnetic (F) and canted antiferromagnetic (CAF)³²⁻³⁵ phases in the $\nu = 0$ state in graphene with armchair-type boundary. Although graphene has a few additional peculiarities (most importantly, the presence of valley degrees of freedom, which makes the QHFM physics richer), there are mathematical and physical similarities to our model. Another related system is a QH bilayer with an

inverted band structure, studied theoretically in Ref. 36. The model Hamiltonian considered in Ref. 36 essentially coincides with the U(1)-symmetric part of our model, but the focus and methods of analysis of Ref. 36 differ from ours in several respects. We point out the analogies between our and these two systems as we move along.

As originally recognized in Ref. 26 for the F phase of the $\nu = 0$ state in graphene with armchair-type boundary, the physics of the edge in the QHFMs at $\nu = 0$ is governed by the fact that the order favored at the edge due to the propagating edge states may be different from that favored in the bulk. This leads to a spatially inhomogeneous OP texture at the edge, which connects the bulk and edge orders. This ground state texture, which can be referred to as the *domain wall*, then determines the properties of the edge excitations.

Since, as already mentioned above, U(1) symmetry will turn out to be crucial for the existence of the TnT phase in this interacting system, in the next Secs. IV-VII we perform the analysis of the U(1)-symmetric model, Eqs. (3.3)-(3.6), and (3.8), and consider the effect of the U(1)-asymmetric terms (3.9) and (3.10) afterwards in Sec. VII C.

IV. BULK PHASE DIAGRAM

In this section, we obtain the bulk mean-field phase diagram for the U(1)-symmetric model [Eqs. (3.3)-(3.6), and (3.8)] completely neglecting the edge [boundary condition (3.8)]. It is obtained by minimizing the energy function $\mathcal{E}(n_z)$ [Eq. (3.6)]. The minimum isospin configuration will be denoted as \mathbf{n}^∞ and referred to as the *bulk ground state*. The minimal energy will be denoted as

$$\mathcal{E}^\infty \equiv \mathcal{E}(n_z^\infty = \cos \theta^\infty) = \min_{n_z} \mathcal{E}(n_z). \quad (4.1)$$

In the case $u > 0$ of the easy-plane anisotropy we consider, minimization of $\mathcal{E}(n_z)$ within the interval $-1 \leq n_z \leq 1$ gives the following phases

$$\mathbf{n}^\infty = \mathbf{n}_z = (0, 0, 1), \quad u < h_z, \quad (4.2)$$

$$\mathbf{n}^\infty = \mathbf{n}^*(\varphi_0) = (\sin \theta^* \cos \varphi_0, \sin \theta^* \sin \varphi_0, \cos \theta^*), \quad -u < h_z < u, \quad (4.3)$$

$$\mathbf{n}^\infty = -\mathbf{n}_z = (0, 0, -1), \quad h_z < -u. \quad (4.4)$$

with the respective energy minima

$$\mathcal{E}^\infty = \mathcal{E}(n_z = +1) = \frac{u}{2} - h_z, \quad u < h_z, \quad (4.5)$$

$$\mathcal{E}^\infty = \mathcal{E}(n_z^*) = -\frac{h_z^2}{2u}, \quad -u < h_z < u, \quad (4.6)$$

$$\mathcal{E}^\infty = \mathcal{E}(n_z = -1) = \frac{u}{2} + h_z, \quad h_z < -u. \quad (4.7)$$

The phases are shown in Fig. 5. The phases $\mathbf{n}^\infty = \pm \mathbf{n}_z$ at $u < h_z$ and $h_z < -u$, respectively, are fully polarized along the direction z of the field h_z . According to the meaning of the isospin, see Eqs. (1.1), (1.2), and (1.3), the $\mathbf{n}^\infty = \pm \mathbf{n}_z$ phases correspond to the occupation of either $|+\mathbf{n}_z\rangle = |a\rangle$ or $|-\mathbf{n}_z\rangle = |b\rangle$ LLs, respectively. The Slater-

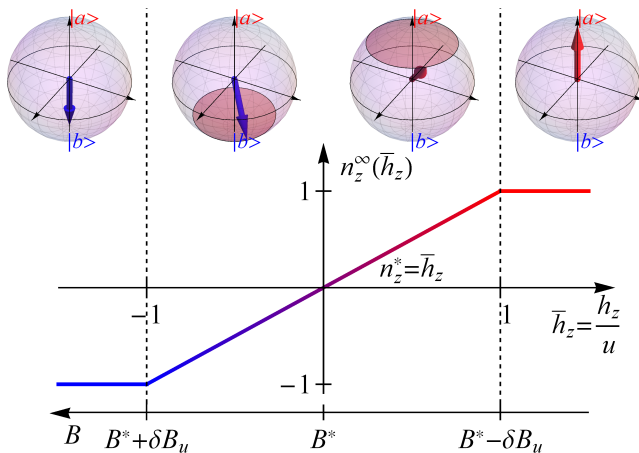


FIG. 5: (Color online) Bulk phase diagram for the U(1)-symmetric σ -model obtained by minimizing the energy function $\mathcal{E}(n_z)$ [Eq. (3.6)]. The plot shows the dependence $n_z^\infty(\bar{h}_z)$ of the optimal isospin projection on the normalized field $\bar{h}_z = h_z/u$; the color code depicts the weight of the a (red) and b (blue) LL states. The Bloch spheres depict the corresponding isospin orders (4.2), (4.3), and (4.4).

determinant ground state $\Psi(\mathbf{n})$ [Eq. (3.1)] in the $\mathbf{n}^\infty = \pm \mathbf{n}_z$ phases is thus the same as in the noninteracting system.

In the “intermediate” phase $\mathbf{n}^\infty = \mathbf{n}^*(\varphi_0)$ at $-u < h_z < u$, the isospin has the optimal projection

$$n_z^* = \cos \theta^* = \bar{h}_z \quad (4.8)$$

on the z direction and arbitrary orientation in the xy plane, parameterized by the angle φ_0 . It is convenient to introduce the dimensionless field

$$\bar{h}_z = \frac{h_z}{u} \quad (4.9)$$

normalized by the anisotropy energy u . Thus, in the intermediate phase, electrons are in a coherent mixture

$$|\mathbf{n}^*(\varphi_0)\rangle = e^{-i\frac{\varphi_0}{2}} \cos \frac{\theta^*}{2} |a\rangle + e^{i\frac{\varphi_0}{2}} \sin \frac{\theta^*}{2} |b\rangle$$

of the two LL states. The appearance of this intermediate phase is the first important distinction from the noninteracting picture.

The U(1) symmetry is thus preserved in the $\mathbf{n}^\infty = \pm \mathbf{n}_z$ phases, but it is spontaneously broken in the intermediate $\mathbf{n}^\infty = \mathbf{n}^*(\varphi_0)$ phase.

The phase transitions at $h_z = \pm u$ are of the second order. According to the dependence (2.9) of $h_z(B)$ on the magnetic field, the transition points $h_z = \pm u$, correspond to the values

$$B^* \mp \delta B_u, \quad \delta B_u \equiv \frac{u}{|\partial_B h_z(B^*)|}, \quad (4.10)$$

of the magnetic field, respectively.

An analogous phase diagram was obtained for a double-layer system³⁶. Also, the region $0 \leq h_z$ reproduces the part of the phase diagram for the $\nu = 0$ state in graphene^{32–34}, where the $\mathbf{n}^\infty = \mathbf{n}_z$ and $\mathbf{n}^\infty = \mathbf{n}^*(\varphi_0)$ phases correspond to the F and CAF phases, respectively. For graphene, the isospin \mathbf{n} would correspond to the spin polarization of one of the sublattices of the honeycomb crystal lattice.

V. SYSTEM WITH AN EDGE, GROUND STATES

In this section, we obtain the ground state configurations of the OP $\mathbf{n}(\mathbf{r})$ taking the effect of the edge into account. Such configurations, to be denoted $\mathbf{n}_0(\mathbf{r})$, minimize the energy functional (3.5),

$$\mathbb{E}[\mathbf{n}_0] = \min_{\mathbf{n}} \mathbb{E}[\mathbf{n}],$$

under the boundary condition (3.8) constraint. The ground state configuration $\mathbf{n}_0(\mathbf{r})$ is a stationary point of the energy functional. In terms of the spherical angles θ and φ [Eq. (1.3)], the stationary-point equations read

$$\frac{\delta \mathbb{E}[\theta, \varphi]}{\delta \theta} = \rho[-\nabla^2 \theta + \frac{1}{2} \sin 2\theta (\nabla \varphi)^2] + \partial_\theta \mathcal{E}(\theta) = 0, \quad (5.1)$$

$$\frac{\delta \mathbb{E}[\theta, \varphi]}{\delta \varphi} = -\rho \nabla (\sin^2 \theta \nabla \varphi) = 0. \quad (5.2)$$

(Throughout, we will denote the energy dependence $\mathcal{E}(\theta) = \mathcal{E}(n_z = \cos \theta)$ on θ by the same function, since it should not lead to confusion.)

Since in the presence of the edge the translational symmetry along y direction is still preserved, the ground state configuration is y -independent, $\mathbf{n}_0(x, y) \equiv \mathbf{n}_0(x)$: changes of the isospin with y would only result in the rise of the gradient energy.

Away from the edge in the bulk, i.e., asymptotically at $x \rightarrow -\infty$, the ground state configurations must approach the constant value

$$\mathbf{n}_0(x \rightarrow -\infty) = \mathbf{n}^\infty \quad (5.3)$$

of the bulk ground state order \mathbf{n}^∞ , which, depending on h_z , is one of the orders (4.2), (4.3), or (4.4) that minimize $\mathcal{E}(n_z)$, as obtained in the previous section. Therefore, whenever \mathbf{n}^∞ differs from the boundary order [Eq. (3.8)]

$$\mathbf{n}_0(x=0) = -\mathbf{n}_z, \quad (5.4)$$

$\mathbf{n}_0(x)$ is a spatially inhomogeneous domain-wall configuration along x that “connects” these orders.

Further, due to the U(1) symmetry of the energy function $\mathcal{E}(n_z)$ and boundary condition (3.8), it is clear that the angle $\varphi(x) \equiv \varphi_0$ in the spherical parametrization (1.3) of $\mathbf{n}_0(x)$ is constant and arbitrary: similarly, changes in φ would only result in the rise of the gradient

energy. Note that Eq. (5.2) is satisfied automatically by a constant φ .

Therefore, the ground state configuration has the following form

$$\mathbf{n}_0(x|\varphi_0) = (\sin \theta_0(x) \cos \varphi_0, \sin \theta_0(x) \sin \varphi_0, \cos \theta_0(x)). \quad (5.5)$$

For the angle $\theta(x)$ dependent only on x and the constant φ_0 , the energy functional (3.5) per unit length in the y direction reduces to

$$E^{1D}[\theta(x); u, h_z] = \int_{-\infty}^0 \frac{dx}{s} E_x[\theta], \quad E_x[\theta] = \frac{\rho}{2} (\nabla_x \theta)^2 + \mathcal{E}(\theta). \quad (5.6)$$

The ground state configuration $\theta_0(x)$ minimizes this functional and thus satisfies its stationary point equation

$$-\rho \nabla_x^2 \theta + \partial_\theta \mathcal{E}(\theta) = 0 \quad (5.7)$$

(which is evidently equivalent to Eq. (5.1) under these assumptions).

Equation (5.7) needs to be supplemented by the boundary conditions

$$\theta(x = -\infty) = \theta^\infty \text{ and } \theta(x = 0) = \pi \quad (5.8)$$

following from Eqs. (5.3) and (5.4), where θ^∞ is the angle of the bulk order \mathbf{n}^∞ .

The solution of this boundary problem can be facilitated by noticing the analogy of Eq. (5.7) with the Newton equation for a point particle in one dimension, where θ and x play the roles of coordinate and time, respectively. The equation has an integral of motion

$$\frac{\rho}{2} (\nabla_x \theta)^2 - \mathcal{E}(\theta) = -\mathcal{E}^\infty, \quad (5.9)$$

equivalent to the total energy of the effective particle. It can be obtained by multiplying Eq. (5.7) by $\nabla_x \theta$ and integrating once over x . The gradient term $\frac{\rho}{2} (\nabla_x \theta)^2$ in Eq. (5.9) plays the role of the kinetic energy, while $-\mathcal{E}(\theta)$ plays the role of the potential energy. The value of this integral of motion is set by its value $-\mathcal{E}^\infty$ in the bulk [Eqs. (4.5), (4.6), and (4.7)], where $\nabla_x \theta \rightarrow 0$.

Equation (5.9) can be further integrated, which produces an implicit dependence of $\theta_0(x)$ on x given by

$$-x = \int_{\theta_0}^{\pi} \frac{d\theta}{\sqrt{\frac{\rho}{2} [\mathcal{E}(\theta) - \mathcal{E}^\infty]}}. \quad (5.10)$$

The functional form (3.6) of $\mathcal{E}(n_z)$ allows for explicit integration of Eq. (5.10) in terms of elementary functions and subsequent inversion. The explicit forms of the solutions are

$$\theta_0(x) = \arccos \left[1 - \frac{2(\bar{h}_z - 1)}{\bar{h}_z \cosh^2(\sqrt{\bar{h}_z - 1} \bar{x}) - 1} \right], \quad u < h_z, \quad (5.11)$$

$$\theta_0(x) = 2 \arctan \left[\sqrt{\frac{1 - \bar{h}_z}{1 + \bar{h}_z}} \frac{1}{\tanh \left(-\frac{\sqrt{1 - \bar{h}_z^2}}{2} \bar{x} \right)} \right], \quad -u < h_z < u, \quad (5.12)$$

$$\theta_0(x) = \pi, \quad h_z < -u. \quad (5.13)$$

Here, \bar{h}_z is the dimensionless field defined in Eq. (4.9) and

$$\bar{x} = \frac{x}{l_u} \quad (5.14)$$

is the dimensionless coordinate normalized by the length scale

$$l_u = \sqrt{\frac{\rho}{u}} \quad (5.15)$$

set by the anisotropy energy u . The solutions, therefore, have the scaling form $\theta_0(x) = \theta_0(x; u, h_z) = \theta_0(\bar{x}; \bar{h}_z)$.

These solutions $\theta_0(x)$ minimize the functional $E^{1D}[\theta]$ [Eq. (5.6)] and the respective isospin configurations $\mathbf{n}_0(x|\varphi_0)$ [Eq. (5.5)] minimize the functional $\mathbb{E}[\mathbf{n}]$

[Eq. (3.5)] in the presence of the edge, described by the boundary condition (5.4).

The functions are plotted in Fig. 6. In the $\mathbf{n}^\infty = \mathbf{n}_z$ and $\mathbf{n}^\infty = \mathbf{n}^*(\varphi_0)$ phases, $\theta_0(x)$ grows monotonically from the bulk value θ^∞ at $x = -\infty$ to π at the edge $x = 0$. Since θ^∞ corresponds to the minimum of $\mathcal{E}(\theta)$ the effective particle starts at “time” $x = -\infty$ at the maximum $-\mathcal{E}^\infty$ of its potential energy $-\mathcal{E}(\theta)$, i.e., in an unstable equilibrium position, and “falls down” the potential energy curve. In the $\mathbf{n}^\infty = -\mathbf{n}_z$ phase, the bulk and edge orders are the same and $\theta_0(x) \equiv \pi$ is a constant.

The solutions $\theta_0(x)$ approach the asymptotic bulk value θ^∞ exponentially over the length scales

$$\frac{l_u}{\sqrt{\bar{h}_z - 1}} = \sqrt{\frac{\rho}{h_z - u}}, \quad u < h_z,$$

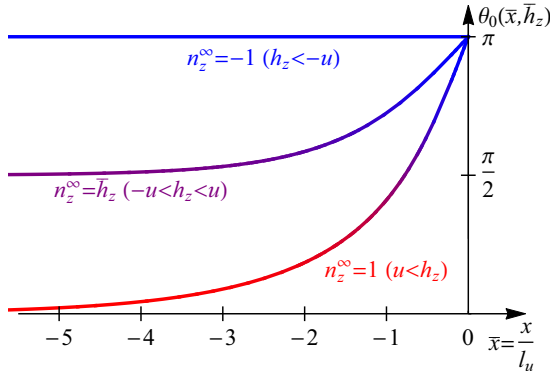


FIG. 6: (Color online) The angle functions $\theta_0(x) = \theta_0(\bar{x}, \bar{h}_z)$ [Eqs. (5.11), (5.12), and (5.13)] for the ground state solution (5.5) for a system with an edge. Three cases according to the three phases [Eqs. (4.2), (4.3), and (4.4)] are shown. At $x \rightarrow -\infty$, the solutions approach the asymptotic values $\theta^\infty(\bar{h}_z)$ for the bulk ground states. At $x = 0$, the solutions satisfy the boundary condition (5.8) imposed by the edge. The functions are color-coded according to the $n_z = \cos \theta_0(x)$ projection, depicting the weight of the a (red) and b (blue) LL states.

$$\frac{l_u}{\sqrt{1 - \bar{h}_z^2}} = \sqrt{\frac{\rho u}{u^2 - \bar{h}_z^2}}, \quad -u < h_z < u. \quad (5.16)$$

At both phase transitions $h_z = \pm u$, these length scales become infinite.

Exactly at the $h_z = u$ phase transition, the solution takes the form

$$\theta_0(x) = 2 \arctan\left(-\frac{1}{\bar{x}}\right), \quad h_z = u, \quad (5.17)$$

as follows from both Eqs. (5.11) and (5.12) in the limits $h_z \rightarrow u \pm 0$. It approaches the bulk value $\theta^\infty = 0$ as a power law $\theta_0(x) \approx -2/\bar{x}$. We emphasize that even exactly at the phase transition $h_z = u$, the domain wall has the spatial scale l_u , although the bulk asymptotic value is approached according to a power law, and not exponentially. This point will be important for the considerations below in Sec. VI D.

Close to the $h_z = -u$ transition, when $h_z + u \ll u$, the bulk value θ^∞ is close to π , and the solution simplifies to

$$\theta_0(x) = \pi - \sqrt{2(1 + \bar{h}_z)} \tanh\left(-\sqrt{\frac{1 + \bar{h}_z}{2}} \bar{x}\right).$$

Most important for topological properties are, however, the degeneracies of the isospin solutions $\mathbf{n}_0(x|\varphi_0)$ [Eq. (5.5)]. According to the possible bulk phases, we have the following three cases.

1) In the $\mathbf{n}^\infty = \mathbf{n}_z$ phase realized at $u < h_z$ [Eq. (4.2)], the ground state solution $\mathbf{n}_0(x|\varphi_0)$ is degenerate according to the arbitrary angle φ_0 . Note though that the bulk order is nondegenerate since at $\mathbf{n}^\infty = \mathbf{n}_z$ the angle φ_0 is undefined and the U(1) symmetry is not spontaneously broken in the bulk. So, this degeneracy occurs (at the mean-field level) at the edge and not in the bulk.

2) In the $\mathbf{n}^\infty = \mathbf{n}^*(\varphi_0)$ phase realized at $-u < h_z < u$ [Eq. (4.3)], the ground state configuration $\mathbf{n}_0(x|\varphi_0)$ is degenerate according to the arbitrary angle φ_0 , equal to the one of the asymptotic bulk configuration $\mathbf{n}^*(\varphi_0)$. So, this degeneracy describes the spontaneous breaking of U(1) symmetry in the bulk and there is not extra degeneracy at the edge.

3) In the $\mathbf{n}^\infty = -\mathbf{n}_z$ phase realized at $h_z < -u$ [Eq. (4.4)], the bulk and edge orders are exactly the same, and the ground state solution for the system with an edge is a constant $\mathbf{n}_0(x) \equiv -\mathbf{n}_z$ and thus nondegenerate (φ_0 is undefined).

The properties can also be illustrated with the help of the Bloch sphere, see Fig. 8. The ground state domain wall configurations $\mathbf{n}_0(x|\varphi_0)$ can be visualized as geodesic paths connecting the bulk \mathbf{n}^∞ and edge $-\mathbf{n}_z$ orders and parameterized by the coordinate x . In the $\mathbf{n}^\infty = \mathbf{n}_z$ phase, the bulk and edge orientations are exactly opposite, and there is an infinite number of geodesics, parameterized by the angle φ_0 . In the $\mathbf{n}^\infty = \mathbf{n}^*(\varphi_0)$ phase, for a given angle φ_0 in the bulk, the geodesic connecting \mathbf{n}^* and $-\mathbf{n}_z$ is unique: it is a path in the vertical plane of the constant φ_0 . As we show in the next Sec. VI, these degeneracy properties of the ground state solutions are key to the properties of the charge edge excitations.

We calculate the ground state energy of the system with an edge. It is sensible to subtract the asymptotic bulk contribution and thus define the energy quantities

$$dE^{1D}[\theta(x); u, h_z] \equiv \int_{-\infty}^0 \frac{dx}{s} dE_x[\theta(x); u, h_z] = E^{1D}[\theta(x); u, h_z] - E^{1D\infty}(u, h_z), \quad (5.18)$$

$$dE_x[\theta(x); u, h_z] \equiv E_x[\theta(x); u, h_z] - \mathcal{E}^\infty(u, h_z), \quad (5.19)$$

$$E^{1D\infty}(u, h_z) \equiv \int_{-\infty}^0 \frac{dx}{s} \mathcal{E}^\infty(u, h_z)$$

in terms of Eq. (5.6). The corresponding ground-state energy per unit length in the y direction equals

$$dE_0^{1D}(u, h_z) \equiv \min_{\theta(x)} dE^{1D}[\theta(x); u, h_z] = dE^{1D}[\theta_0(x; u, h_z); u, h_z] \quad (5.20)$$

and can be referred to as the *domain-wall energy*. This quantity is not extensive in the x direction and indeed describes the energy associated only with the domain-wall isospin texture at the edge.

Exploiting the integral of motion (5.9), the domain-wall energy can be presented as

$$dE_0^{1D}(u; h_z) = 2 \int_{-\infty}^0 \frac{dx}{s} [\mathcal{E}(\theta_0(x)) - \mathcal{E}^\infty]$$

and calculated explicitly using the expressions (5.11) and (5.12) for the ground state solutions. For the $\mathbf{n}^\infty = \mathbf{n}_z$ phase [the same can be done for the $\mathbf{n}^\infty = \mathbf{n}_0^*(\varphi)$ phase], we obtain

$$dE_0^{1D}(u, h_z) = 2 \frac{h_z}{s} u F(\bar{h}_z), \quad (5.21)$$

where

$$F(\bar{h}_z) = -F_2(\bar{h}_z) + \bar{h}_z F_1(\bar{h}_z) = \bar{h}_z \arcsin \frac{1}{\sqrt{\bar{h}_z}} + \sqrt{\bar{h}_z - 1}, \quad u < h_z, \quad (5.22)$$

$$F_2(\bar{h}_z) = \frac{1}{2} \int_{-\infty}^0 d\bar{x} \sin^2 \theta_0(\bar{x}) = \bar{h}_z \arcsin \frac{1}{\sqrt{\bar{h}_z}} - \sqrt{\bar{h}_z - 1}, \quad (5.23)$$

$$F_1(\bar{h}_z) = \int_{-\infty}^0 d\bar{x} [1 - \cos \theta_0(\bar{x})] = 2 \arcsin \frac{1}{\sqrt{\bar{h}_z}} \quad (5.24)$$

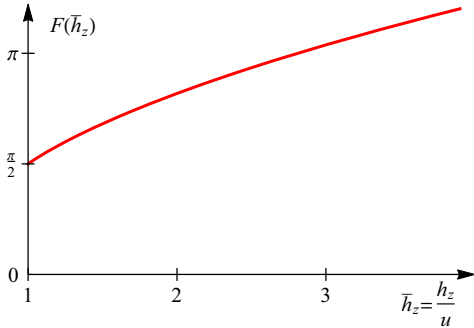


FIG. 7: (Color online) The function $F(\bar{h}_z)$ [Eq. (5.22)], which determines the dependence of the ground-state domain-wall energy $dE_0^{1D}(u, h_z)$ [Eq. (5.21)] on the normalized field $\bar{h}_z = h_z/u$ in the $\mathbf{n}^\infty = \mathbf{n}_z$ phase at $u < h_z$.

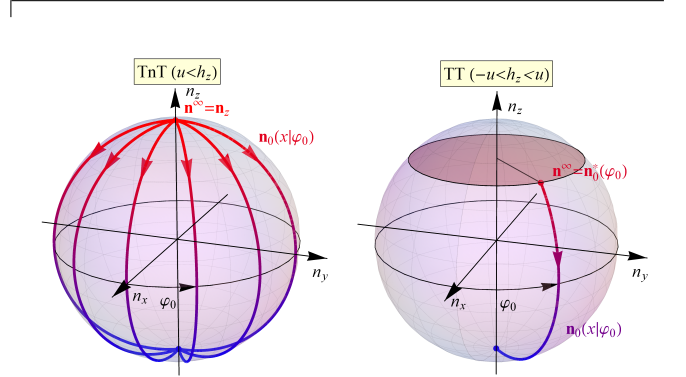


FIG. 8: (Color online) The ground state geodesic paths $\mathbf{n}_0(x|\varphi_0)$ [Eq. (5.5)] on the isospin Bloch sphere for the $\mathbf{n}^\infty = \mathbf{n}_z$ (left) and $\mathbf{n}^\infty = \mathbf{n}_0^*(\varphi_0)$ (right) phases, realized at $u < h_z$ and $-h_z < u < h_z$, respectively.

are dimensionless functions of the normalized field \bar{h}_z , the latter two arising from the anisotropy $\frac{u}{2}(n_z^2 - 1)$ and "Zeeman" $-h_z(n_z - 1)$ contributions to $\mathcal{E}(\theta_0(x)) - \mathcal{E}^\infty$, respectively. The function $F(\bar{h}_z)$ is plotted in Fig. 14.

Importantly, as we will see below in Secs. VIB and VII, the dependence (5.21) of the domain-wall energy on parameters u and h_z defines not only the ground state but also the properties of the low-energy edge excitations of the $\mathbf{n}^\infty = \mathbf{n}_z$ phase.

VI. SYSTEM WITH AN EDGE, CHARGE EXCITATIONS

A. General considerations

Having established the properties of the ground states of the system with an edge, we now turn to the analysis of its charge excitations.

As is well-known²⁵, QHFM systems support charge excitations, which are described by the configurations of the OP with nonzero topological charge, equal to the electric

charge. For the system in question, with the OP being the isospin- $\frac{1}{2}$, the charge density of a configuration $\mathbf{n}(\mathbf{r})$ is given by

$$\begin{aligned}\kappa[\mathbf{n}](\mathbf{r}) &= \frac{1}{4\pi}(\mathbf{n} \cdot [\nabla_x \mathbf{n} \times \nabla_y \mathbf{n}]) \\ &= \frac{1}{4\pi} \sin \theta (\nabla_x \theta \nabla_y \varphi - \nabla_y \theta \nabla_x \varphi).\end{aligned}\quad (6.1)$$

The total net charge of the configuration is then given by the integral

$$q[\mathbf{n}] = \int d^2\mathbf{r} \kappa[\mathbf{n}](\mathbf{r}).\quad (6.2)$$

This topological charge is the invariant of the mapping realized by $\mathbf{n}(\mathbf{r})$ from the coordinate space of \mathbf{r} to the 2D Bloch sphere; it can be visualized as the number of times the sphere is wound as the space of \mathbf{r} is explored. In this article, we will be interested in the excitations with integer charge q , whose boundary values are the same as in the ground state. In principle, excitations with non-integer charge q are also possible if the ground state has broken continuous symmetry, which is indeed the case for the intermediate phase $\mathbf{n}^\infty = \mathbf{n}^*(\varphi_0)$, but they are outside of the scope of this paper.

The difference

$$\delta\mathbb{E}[\mathbf{n}] \equiv \mathbb{E}[\mathbf{n}] - \mathbb{E}[\mathbf{n}_0]\quad (6.3)$$

between the energy of a configuration $\mathbf{n}(\mathbf{r})$ and of the ground state configuration $\mathbf{n}_0(x)$ will be called the *excitation energy* of $\mathbf{n}(\mathbf{r})$. The configuration $\mathbf{n}^q(\mathbf{r})$ of charge q will be further designated with a superscript. Denote $\mathbf{n}_0^q(\mathbf{r})$ the charge- q configuration that minimizes the energy (3.5) among all charge- q configurations $\mathbf{n}^q(\mathbf{r})$,

$$\mathbb{E}[\mathbf{n}_0^q] = \min_{\mathbf{n}^q} \mathbb{E}[\mathbf{n}^q].\quad (6.4)$$

Clearly, the ground state configuration $\mathbf{n}_0(x|\varphi_0)$ has zero charge (the charge density $\kappa[\mathbf{n}_0] \equiv 0$) and hence $\mathbf{n}_0 = \mathbf{n}_0^{q=0}$.

The excitation energy (6.3)

$$\Delta^q \equiv \min_{\mathbf{n}^q} \delta\mathbb{E}[\mathbf{n}^q] = \delta\mathbb{E}[\mathbf{n}_0^q] = \mathbb{E}[\mathbf{n}_0^q] - \mathbb{E}[\mathbf{n}_0]\quad (6.5)$$

of the minimal-energy configuration $\mathbf{n}_0^q(\mathbf{r})$ will be called the *gap* of charge- q excitations. The minimum

$$\Delta = \min_{q \neq 0} \Delta^q$$

among all $q \neq 0$ defines the gap of excitations of any charge. Typically, Δ^q is a growing function of q , and therefore the unit-charge $q = \pm 1$ excitations, for which the Bloch sphere is covered once, determine the gap, $\Delta = \Delta^{q=\pm 1}$.

The minimal-energy charge- q configurations $\mathbf{n}_0^q(\mathbf{r})$ satisfy the same stationary-point Eqs. (5.1) and (5.2) as the ground state $\mathbf{n}_0(x|\varphi_0)$, since they describe any *local* minimum in the configuration space. In order not to contain ‘‘extensive’’ contributions to the excitation energy (6.5), proportional to the size of the system, the configurations $\mathbf{n}_0^q(\mathbf{r})$ must asymptotically approach the ground state configuration $\mathbf{n}_0(x|\varphi_0)$:

$$\mathbf{n}_0^q(x, y \rightarrow \pm\infty) \rightarrow \mathbf{n}_0(x|\varphi_0),$$

$$\mathbf{n}_0^q(x \rightarrow -\infty, y) \rightarrow \mathbf{n}^\infty.$$

The finite-size region, where most of the winding of the Bloch sphere occurs, $\mathbf{n}_0^q(\mathbf{r})$ differs from $\mathbf{n}_0(x|\varphi_0)$, and the charge density $\kappa[\mathbf{n}_0^q](\mathbf{r})$ is located, can be referred to as the *core* of the charge excitation.

For the considered system with an edge, one should distinguish between bulk and edge charge excitations. In the bulk excitations, known as skyrmions, the core is located deep in the bulk, away from the domain wall at the edge, such that its effect can be neglected. In the edge excitations, the core is located in the domain wall. At the qualitative level, it is clear that the energy of the edge charge excitation will generally be smaller than that of the bulk skyrmion: since in the ground state $\mathbf{n}_0(x|\varphi_0)$ some changes in the isospin orientation are already present, less additional changes are required in $\mathbf{n}_0^q(\mathbf{r})$ to wind the whole Bloch sphere; hence, the smaller the energy cost. The general properties of bulk skyrmions are well-understood²⁵; below, we concentrate on the edge excitations.

B. Gapless edge excitations of the $\mathbf{n}^\infty = \mathbf{n}_z$ phase

We first look at the $\mathbf{n}^\infty = \mathbf{n}_z$ phase with preserved U(1) symmetry in the bulk.

According to the previous section, in the $\mathbf{n}^\infty = \mathbf{n}_z$ phase, the bulk isospin orientation is exactly opposite to the edge isospin orientation and there is an infinite number of geodesics $\mathbf{n}_0(x|\varphi_0)$, parameterized by the angle φ_0 , connecting these two orientations, see Fig. 8. This degeneracy allows one to construct a charge excitation by winding the angle φ_0 in the y direction along the edge^{26,30}. In fact, the Ansatz $(\theta(x), \varphi(y))$ for $\mathbf{n}(\mathbf{r})$ [Eq. (1.3)] decouples the stationary point equations (5.1) and (5.2). Equation (5.2) reduces to

$$-\nabla_y^2 \varphi(y) = 0.\quad (6.6)$$

Introducing the sample boundaries along the y direction at $y = \pm \frac{L_y}{2}$ and imposing the periodic boundary condition

$$\mathbf{n}(x, y = +\frac{L_y}{2}) = \mathbf{n}(x, y = -\frac{L_y}{2}),$$

for the solution to Eq. (6.6), we obtain

$$\varphi_0^q(y) = \varphi_0 + 2\pi q \frac{y}{L_y}, \quad \nabla_y \varphi_0^q = \frac{2\pi q}{L_y}, \quad u < h_z,\quad (6.7)$$

where q is integer. The integer q is indeed the topological charge of the configuration, as can be confirmed from either the geometric considerations or explicit calculation according to Eqs. (6.1) and (6.2).

The energy functional then becomes

$$\mathbb{E}[\theta(x), \varphi_0^q(y)] = L_y \int_{-\infty}^0 \frac{dx}{s} \left\{ \frac{\rho}{2} [(\nabla_x \theta)^2 + \sin^2 \theta (\nabla_y \varphi_0^q)^2] + \mathcal{E}(\theta(x)) \right\} = L_y \{ dE^{1D}[\theta(x); u - \rho(\nabla_y \varphi_0^q)^2, h_z] + E^{1D\infty} \}. \quad (6.8)$$

We notice that the gradient term $\frac{\rho}{2} \sin^2 \theta (\nabla_y \varphi_0^q)^2$ has the form of the anisotropy energy $\frac{u}{2} (n_z^2 - 1)$ and the functional (6.8) thus has the same form as the one (5.6) for the ground state with the redefined anisotropy energy $u - \rho(\nabla_y \varphi_0^q)^2$ and can be expressed in terms of the quantities in Eq. (5.18). Therefore, the functional (6.8)

is minimized by the modified ground state configuration [Eq. (5.11)]

$$\theta_0^q(x) = \theta_0(x; u - \rho(\nabla_y \varphi_0^q)^2, h_z), \quad u < h_z, \quad (6.9)$$

and the gap (6.5)

$$\Delta^q = L_y \left[dE_0^{1D}(u - \rho(2\pi q/L_y)^2, h_z) - dE_0^{1D}(u, h_z) \right], \quad u < h_z, \quad (6.10)$$

of charge- q edge excitations of the $\mathbf{n}^\infty = \mathbf{n}_z$ phase is expressed exactly in terms of the domain-wall energy (5.21).

The isospin configuration of the charge- q excitation in the $\mathbf{n}^\infty = \mathbf{n}_z$ phase has the form

$$\mathbf{n}_0^q(x, y) = (\sin \theta_0^q(x) \cos \varphi_0^q(y), \sin \theta_0^q(x) \sin \varphi_0^q(y), \cos \theta_0^q(x)), \quad u < h_z, \quad (6.11)$$

and is shown in Fig. 9.

The gap (6.10) is finite only due to the finite size L_y of the sample in the y direction and vanishes in the limit $L_y \rightarrow \infty$. Therefore, the phase $\mathbf{n}^\infty = \mathbf{n}_z$ supports gapless edge charge excitations, similar to the findings of Refs. 26,30. The leading term in the large-size limit $L_y \rightarrow \infty$ can be obtained as an expansion

$$\begin{aligned} \Delta^q &\approx -L_y \partial_u dE_0^{1D}(u, h_z) \rho \left(\frac{2\pi q}{L_y} \right)^2 \\ &= (2\pi q)^2 \frac{l_u}{L_y} F_2(\bar{h}_z) \varepsilon_\odot \sim q^2 \frac{l_u}{L_y} \varepsilon_\odot, \quad u < h_z \end{aligned} \quad (6.12)$$

Here,

$$\varepsilon_\odot \equiv \frac{\rho}{s} \sim \frac{e_*^2}{l} \quad (6.13)$$

is the energy associated with the gradient term; it is due to SU(2)-symmetric interactions and is thus set by the Coulomb energy. Equation (6.12) can also be obtained in a simpler way, approximating $\theta_0^q(x) \approx \theta_0(x; u, h_z)$ [Eq. (6.9)] by the ground state configuration (5.11), i.e. taking $\mathbf{n}_0^q(\mathbf{r}) \approx \mathbf{n}_0(x|\varphi_0^q(y))$, in which case the gap contains only the gradient term

$$\Delta^q \approx \int \frac{d^2 \mathbf{r}}{s} \frac{\rho}{2} \sin^2 \theta_0(x) (\nabla \varphi_0^q(y))^2, \quad (6.14)$$

which does agree with Eq. (6.12).

C. Gapped edge excitations of the $\mathbf{n}^\infty = -\mathbf{n}_z$ and $\mathbf{n}^\infty = \mathbf{n}^*(\varphi_0)$ phases

The above construction of the gapless charge excitations in the $\mathbf{n}^\infty = \mathbf{n}_z$ phase is possible due to two conditions realized *in the ground state* $\mathbf{n}_0(x|\varphi_0)$: (i) preserved U(1) symmetry in the bulk and (ii) continuous degeneracy of the ground state solution at the edge. In the other two phases, one of these conditions is violated. In the intermediate phase $\mathbf{n}^\infty = \mathbf{n}^*(\varphi_0)$ [Eq. (4.3)], the U(1) symmetry is spontaneously broken in the bulk and, *for a given bulk order*, characterized by the angle φ_0 , the ground state solution $\mathbf{n}_0(x|\varphi_0)$ is unique. In the $\mathbf{n}^\infty = -\mathbf{n}_z$ phase [Eq. (4.4)], the U(1) symmetry is preserved in the bulk, but the bulk and edge orientations are exactly the same and the ground state solution is just a constant $\mathbf{n}_0(x) \equiv -\mathbf{n}_z$. These crucial differences in the ground state edge configurations of the phases are visualized in Fig. 8. As a result, in both phases, the ground state solution is unique for a given bulk order and analogous construction of the gapless charge excitations is not possible. The edge charge excitations are therefore gapped. In the intermediate $\mathbf{n}^\infty = \mathbf{n}_0(\varphi_0)$ phase, the typical edge charge configuration $\mathbf{n}_0^1(\mathbf{r})$ has the form shown in Fig. 10, as we also demonstrate numerically, see Sec. VI E.

In fact, in the phase $\mathbf{n}^\infty = -\mathbf{n}_z$, the lowest energy integer-charge excitations are the bulk skyrmions, with the core infinitely far (relative to its size) away from the edge. This can be understood from the following argument. The *bulk* skyrmions are the minimal-energy

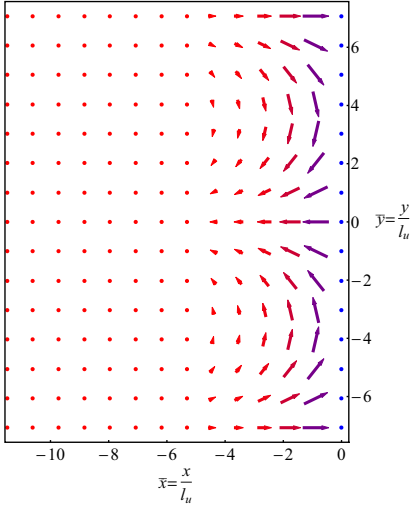


FIG. 9: (Color online) The unit-charge isospin configuration $\mathbf{n}_0^1(\mathbf{r})$ [Eqs. (6.7), (6.9), and (6.11)] in the TnT $\mathbf{n}^\infty = \mathbf{n}_z$ phase with preserved U(1) symmetry at $u < h_z$. The arrows depict the 2D components $(n_x(\mathbf{r}), n_y(\mathbf{r}))$, while the red-blue color code represents the value of the $n_z(\mathbf{r})$ component, in accord with Figs. 5 and 6. The paths on the Bloch sphere for varying $-\infty < x \leq 0$ and several constant values of y are shown in Fig. 8(left).

configurations in an *infinite* sample among all charged configurations with the constraint $\mathbf{n}(r \rightarrow \infty) = -\mathbf{n}_z$. For the half-infinite sample, when the boundary condition $\mathbf{n}(x = 0, y) = -\mathbf{n}_z$ [Eq. (3.8)] is imposed, one can continue the half-plane configurations to the whole plane with the constraint $\mathbf{n}(x > 0, y) = -\mathbf{n}_z$ in the other half-plane. This would constrain the possible set of configurations, which can only result in an increase of the excitation energy compared to that of the bulk skyrmions, for which such a constraint is absent. In other words, placing the core closer to the edge in this case can only result in an energetically less favorable configuration. Therefore, the $\mathbf{n}^\infty = -\mathbf{n}_z$ phase has the largest energy of charge excitations among all three phases, given by that of the bulk skyrmion,

$$\Delta^q = \Delta_{\text{sk}}^q, \quad h_z < -u. \quad (6.15)$$

When the term (higher order in gradients) describing the Coulomb self-interaction of the charge density $\kappa[\mathbf{n}](\mathbf{r})$ [Eq. (6.1)] is neglected, as done in the σ -model we study, the skyrmion energy is given by

$$\Delta_{\text{sk}}^q = 4\pi\varepsilon_\circ|q| \quad (6.16)$$

and its size is formally zero³⁷ due to the presence of the energy $\mathcal{E}(n_z)$ of the SU(2)-asymmetric terms.

The general qualitative behavior of the edge charge excitation gap $\Delta^q(h_z)$ (6.5) in the intermediate $\mathbf{n}^\infty = \mathbf{n}^*(\varphi_0)$ phase can be understood from the continuity argument. Since the transitions at $h_z = \pm u$ are continuous second-order transitions and the intermediate phase

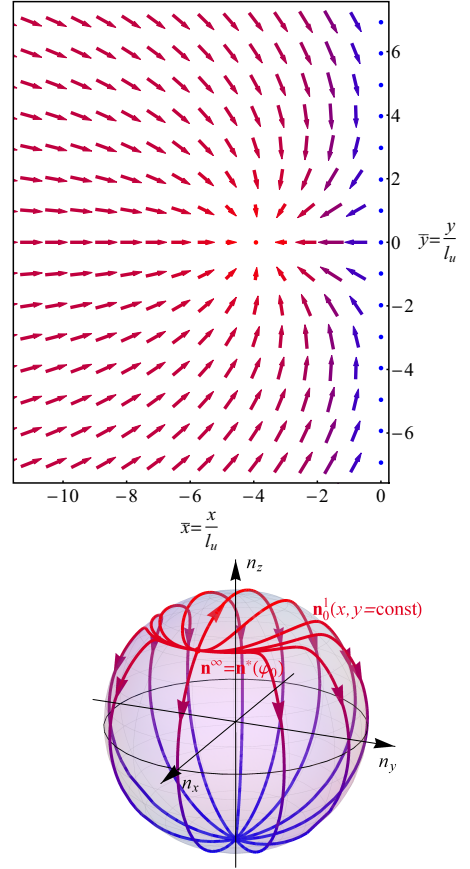


FIG. 10: (Color online) The isospin unit-charge configuration $\mathbf{n}_0^1(\mathbf{r})$ in the TT $\mathbf{n}^\infty = \mathbf{n}^*(\varphi_0)$ phase with spontaneously broken U(1) symmetry at $-u < h_z < u$, obtained numerically for $\bar{h}_z = 0.5$ (top) and $\bar{h}_z = 0.75$ (bottom). (top) The arrows depict the 2D components $(n_x(\mathbf{r}), n_y(\mathbf{r}))$, while the red-blue color code represents the value of the $n_z(\mathbf{r})$ component. (bottom) The paths on the Bloch sphere $\mathbf{n}_0^1(x, y)$ for varying $-\infty < x \leq 0$ and several constant values of y .

continuously interpolates between the $\mathbf{n}^\infty = \mathbf{n}_z$ and $\mathbf{n}^\infty = -\mathbf{n}_z$ phases, $\Delta^q(h_z)$ monotonically and continuously grows upon decreasing h_z in the range $-u < h_z < u$, starting from zero value at $h_z = u$ and reaching its maximal value of Δ_{sk}^q at $h_z = -u$. Since the bulk phase is controlled solely by the normalized dimensionless field \bar{h}_z [Eq. (4.9)], the gap has the following scaling form

$$\Delta^q(h_z) = \varepsilon_\circ \bar{\Delta}^q(\bar{h}_z),$$

where $\bar{\Delta}^q(\bar{h}_z)$ is a dimensionless function of \bar{h}_z .

An analogous continuous growth of the edge excitation gap was earlier predicted for the CAF phase of the $\nu = 0$ state in graphene, originally employing a similar continuity argument³⁴ and within a simplified picture of single-particle edge excitations³⁵. The transport behavior well consistent with this scenario was shortly after observed in both bilayer³⁸ and monolayer²⁰ graphene. More recently, an analytical estimate for the edge excitation gap of the CAF phase was obtained²⁷ within a low-energy theory

approach analogous to the one employed here; the estimate we make below is in accord with that result.

D. Intermediate phase close to the phase transition

$h_z = u$

In the intermediate phase $\mathbf{n}^\infty = \mathbf{n}^*(\varphi_0)$ close to the phase transition $h_z = u$, i.e., when the deviation

$$\delta\bar{h}_z = \frac{\delta h_z}{u} = \bar{h}_z - 1, \quad \delta h_z = h_z - u \quad (6.17)$$

is negative and small, $|\delta\bar{h}_z| \ll 1$, the gap $\bar{\Delta}^q(\bar{h}_z) \ll 1$ is also small and can be estimated analytically.

First, by analogy with the construction for the $\mathbf{n}^\infty = \mathbf{n}_z$ phase, consider the configuration $\mathbf{n}_0(x|\varphi^q(y))$ obtained from the ground state configuration [Eqs. (5.5) and (5.12)] for the intermediate phase by slowly (i.e., at scales much larger than the domain-wall width l_u) winding the angle $\varphi^q(y)$ q times as the y direction is spanned. The shape of $\varphi^q(y)$ is to be optimized. The excitation energy $\delta\mathbb{E}[\mathbf{n}_0(x|\varphi^q(y))]$ [Eq. (6.3)] of such a configuration would also contain only the gradient contribution, analogous to Eq. (6.10). However, since, unlike the $\mathbf{n}^\infty = \mathbf{n}_z$ phase, the bulk asymptotic angle $\theta^\infty = \theta^* \neq 0$ [Eq. (4.8)] is nonzero in the intermediate phase, the integral $\int_{-\infty}^0 dx \dots$ would not be constrained to the domain-wall region of size l_u , but would also contain an extensive contribution proportional to the size of the sample in the x direction. Besides, due to the winding of $\varphi^q(y)$, the asymptotic value $\mathbf{n}_0(x = -\infty|\varphi^q(y)) = \mathbf{n}^*(\varphi^q(y))$ would differ from that $\mathbf{n}^q(x = -\infty, y) = \mathbf{n}^*(\varphi_0)$ of the bulk ground state. Qualitatively, the charge- q configuration $\mathbf{n}^q(\mathbf{r})$ must have the form shown in Fig. 10 for $q = 1$.

Nonetheless, for a given $\varphi^q(y)$, the energy is still minimized well by the configuration $\mathbf{n}_0(x|\varphi^q(y))$ in the domain-wall region. It is in the bulk region, where the configuration needs to be modified.

The proximity to the phase transition allows one to efficiently separate the domain-wall and bulk contributions as follows. The asymptotic bulk order $\mathbf{n}^\infty = \mathbf{n}^*(\varphi_0)$ deviates only a little from \mathbf{n}_z : from Eq. (4.8), the optimal angle in the bulk ground state is given by

$$\theta^{*2} \approx 2|\delta\bar{h}_z| \ll 1.$$

When the isospin $\mathbf{n}(\mathbf{r})$ is close to \mathbf{n}_z , such that its angle $\theta(\mathbf{r}) \lesssim \theta^*$, the energetics is governed by this smaller scale $|\delta h_z| \ll u$ and the associated spatial scale

$$l_{\delta h_z} \equiv \sqrt{\frac{\rho}{|\delta h_z|}} = \frac{l_u}{\sqrt{|\delta\bar{h}_z|}} \gg l_u$$

is much larger than the domain-wall width l_u [see also Eq. (5.16)].

We choose a length scale x_0 such that

$$l_{\delta h_z} \gg x_0 \gg l_u.$$

Since $x_0 \gg l_u$, the ground state configuration $\mathbf{n}_0(x = -x_0|\varphi_0)$ at $x = -x_0$ is already close to its bulk asymptotic value $\theta_0(x = -x_0) \approx \theta^*$. We emphasize that even exactly at the phase transition $h_z = u$, the domain wall width is l_u , only the bulk value is approached as a power law and not exponentially, see Eq. (5.17). So, for the sought charge- q configuration $\mathbf{n}^q(\mathbf{r})$, we consider the above ground state configuration with the adiabatically changing angle $\varphi^q(y)$ only in the region up to this distance from the edge:

$$\mathbf{n}^q(\mathbf{r}) \approx \mathbf{n}_0(x|\varphi^q(y)), \quad -x_0 < x \leq 0.$$

Due to the other condition $l_{\delta h_z} \gg x_0$, the contribution to the excitation energy from the region $-x_0 < x < 0$ is not extensive and can be approximated as

$$\begin{aligned} \delta\mathbb{E}[\mathbf{n}^q]_{(-x_0, 0)} &= \int_{-x_0 < x < 0} \frac{d^2\mathbf{r}}{s} (E[\mathbf{n}^q] - E[\mathbf{n}_0]) \\ &\approx \#\varepsilon_\odot l_u \int_{-\infty}^{+\infty} dy [\nabla_y \varphi^q(y)]^2. \end{aligned} \quad (6.18)$$

Here and below, $\#$ indicates undetermined numerical factors that are beyond the accuracy of the considered approximation.

In the remaining ‘‘bulk’’ region $x < -x_0$, the configuration $\mathbf{n}^q(\mathbf{r})$ must connect the boundary values $\mathbf{n}^q(x = -\infty, y) = \mathbf{n}^*(\varphi_0)$ and $\mathbf{n}^q(x = -x_0, y) = \mathbf{n}_0(x|\varphi^q(y)) \approx \mathbf{n}^*(\varphi^q(y))$. Since at both boundaries the isospin is close to \mathbf{n}_z , the isospin $\mathbf{n}^q(\mathbf{r})$ is close to \mathbf{n}_z within the whole region, and therefore, according to the above, varies over the spatial scales on the order of $l_{\delta h_z}$ or greater.

In fact, the bulk region $x < -x_0$ ‘‘traps a vortex’’ of charge q (not to be confused with the skyrmion charge): when going along its rectangular boundary, the phase $\varphi^q(x, y)$ winds the circle q times (all at the $x = -x_0$ boundary), while the angle $\theta \approx \theta^*$ remains almost constant. The leading contribution to the energy of such a vortex configuration comes from the region outside of its core – the region where the isospin covers the solid angle $\theta \lesssim \theta^*$. This contribution is logarithmic; to obtain it, one may consider the radial form $\theta(r, \phi) = \theta^*$, $\varphi(r, \phi) = q\phi$, where $\mathbf{r} = r(\cos \phi, \sin \phi)$, relative to the ‘‘center’’ of the vortex in the bulk region $x < -x_0$, the point at which $\mathbf{n}_0^q(\mathbf{r}) = \mathbf{n}_z$ in Fig. 10. This gives

$$\begin{aligned} \delta\mathbb{E}[\mathbf{n}^q]_{(-\infty, -x_0)} &= \int_{x < -x_0} \frac{d^2\mathbf{r}}{s} (E[\mathbf{n}^q] - E[\mathbf{n}_0]) \\ &\approx \int \frac{2\pi r dr}{s} \frac{\rho}{2} \sin^2 \theta (\nabla \varphi)^2 \\ &\approx \int_{|q|l_{\delta h_z}}^l \frac{2\pi r dr}{s} \frac{\rho}{2} \theta^{*2} \frac{q^2}{r^2} \\ &= \frac{2\pi\rho}{s} |\delta\bar{h}_z| q^2 \ln \frac{l}{|q|l_{\delta h_z}}. \end{aligned} \quad (6.19)$$

The lower limit is determined by the size $|q|l_{\delta h_z}$ of the vortex core. In our case, the upper limit $l \gg |q|l_{\delta h_z}$

is set by the distance from the vortex core to the edge. This same scale l has to match the extent of $\varphi^q(y)$ in the domain wall in the y direction (the size of the “winding region”). Estimating $\nabla_y \varphi^q(y) \sim q/l$ and adding the domain-wall (6.18) and bulk (6.19) contributions, for the excitation energy of the so-constructed configuration one obtains

$$\begin{aligned} \delta\mathbb{E}[\mathbf{n}^q] &= \delta\mathbb{E}[\mathbf{n}^q]_{(-\infty, -x_0)} + \delta\mathbb{E}[\mathbf{n}^q]_{(-x_0, 0)} \\ &\approx \varepsilon_{\odot} q^2 \left(2\pi |\delta\bar{h}_z| \ln \frac{l}{|q|l|\delta h_z|} + \# \frac{l_u}{l} \right). \end{aligned} \quad (6.20)$$

The dimension l is the only remaining variational parameter. Minimization of this energy with respect to L yields the leading terms of the asymptotics expansion

$$\bar{\Delta}^q(\bar{h}_z \rightarrow 1 - 0) = \pi q^2 |\delta\bar{h}_z| \ln \frac{C}{q^2 |\delta\bar{h}_z|} + o(|\delta\bar{h}_z|) \quad (6.21)$$

for the gap of charge edge excitations in the intermediate phase $\mathbf{n}^\infty = \mathbf{n}^*(\varphi_0)$ close to the phase transition $h_z = u$. The minimum (6.21) of Eq. (6.20) is reached at the optimal length

$$l^* \equiv \frac{l_u}{|\delta\bar{h}_z|} = \frac{l\delta h_z}{\sqrt{|\delta\bar{h}_z|}}.$$

The numerical factor $C \sim 1$ cannot be determined within the accuracy of the considered logarithmic approximation. For unit charge $q = \pm 1$, the estimate (6.21) agrees with that of Ref. 27.

E. Numerical calculations

We also confirm the above-presented behavior by calculating the unit-charge $q = 1$ edge excitations numerically. The configurations $\mathbf{n}_0^1(\mathbf{r})$ that deliver the energy minimum (6.4) within the $q = 1$ sector are found by solving the discretized version of the stationary-point Eqs. (5.1) and (5.2). We solve them using a variant of the multi-grid relaxation methods for boundary value problems³⁹. The calculations are performed for a finite-size system $(x, y) \in (-L_x, 0) \times (-\frac{L_y}{2}, +\frac{L_y}{2})$ with dimensions L_x and L_y . For all sizes L_y indicated in Fig. 11, except the largest one $(L_x, L_y) = (120, 160)\sqrt{2}l_u$, we considered square samples with $L_x = L_y$. The gap $\bar{\Delta}^1(\bar{h}_z)$ is calculated using a discretized version of Eq. (6.5). The plots for the gap $\bar{\Delta}^1(\bar{h}_z)$ as a function of the normalized field \bar{h}_z for several different system dimensions $L_{x,y}/l_u$ are presented in Fig. 11.

In the region $u < h_z$ of the $\mathbf{n}^\infty = \mathbf{n}_z$ phase, the numerically calculated gap $\bar{\Delta}^1(\bar{h}_z)$ accurately agrees with the exact analytic dependence (6.10) on \bar{h}_z and L_y , thus confirming that the edge charge excitations are gapless in the infinite-size limit $L_y \rightarrow \infty$. The typical edge charge configuration $\mathbf{n}_0^1(\mathbf{r})$ in the $\mathbf{n}^\infty = \mathbf{n}_z$ phase has the form shown Fig. 9, in full agreement with the analytical expressions (6.7), (6.9), and (6.11).

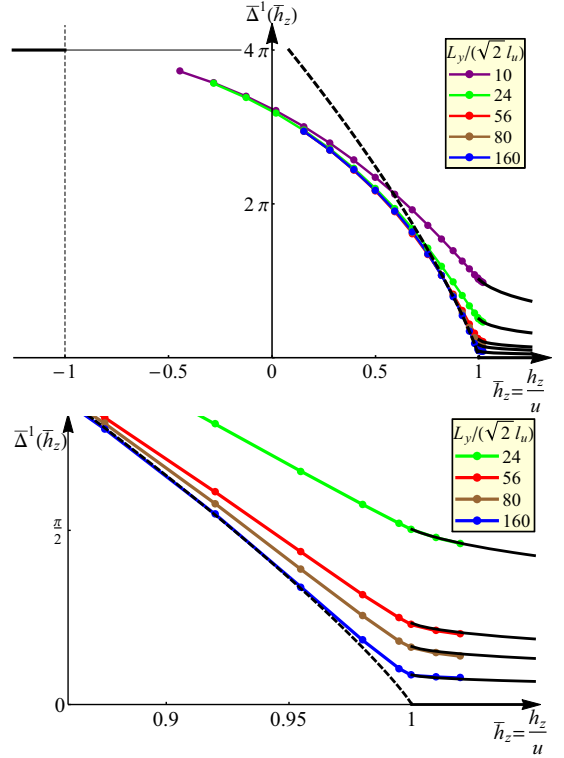


FIG. 11: (Color online) (top) The dependence of the gap $\bar{\Delta}^1(\bar{h}_z)$ of the edge charge excitations $\mathbf{n}_0^1(\mathbf{r})$ on the normalized field \bar{h}_z , calculated numerically for various sample sizes. The black solid lines in the $1 < \bar{h}_z$ region are the exact gap dependencies (6.10) for a finite-size system. The black horizontal solid line in the $-1 < \bar{h}_z$ region is the analytic value (6.16) of the gap, given by the energy of a free skyrmion. The black dashed line in the $-1 < \bar{h}_z < 1$ region is the asymptotic gap dependence (6.21) with the fitted parameter $\ln C = 4.27$. (bottom) Zoomed-in region around the phase transition point $\bar{h}_z = 1$.

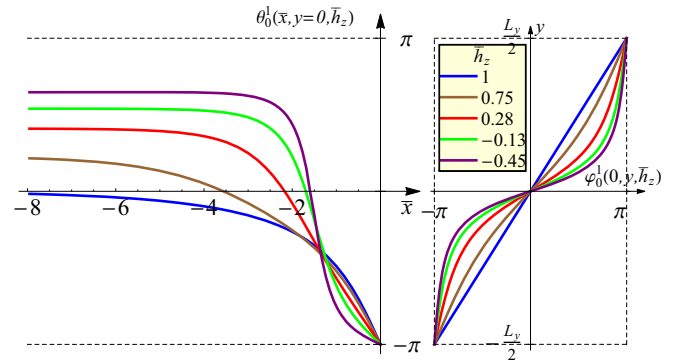


FIG. 12: (Color online) The angle functions $\theta_0^1(x, y=0)$ and $\varphi_0^1(x=-0, y)$ of the unit-charge edge configurations $\mathbf{n}_0^1(\mathbf{r})$ in the intermediate phase $\mathbf{n}^\infty = \mathbf{n}^*(\varphi_0)$ at $-u < h_z < u$, obtained numerically for $L_x = L_y = 10\sqrt{2}l_u$ sample for various values of h_z . The size of the configuration decreases with decreasing h_z .

In the region $-u < h_z < u$ of the intermediate phase $\mathbf{n}^\infty = \mathbf{n}^*(\varphi_0)$, the gap becomes independent of the sample dimensions $L_{x,y}$, as they become larger than the size of the configuration. Close to the transition point $h_z = u$ in the intermediate phase, for large enough $L_{x,y}/l_u$, the numerical data points fit to the analytical estimate (6.21): for the largest-size sample $(L_x, L_y) = (120, 160)\sqrt{2}l_u$ (with the smallest size effects), fitting to the data points $(\bar{h}_z, \bar{\Delta}^1(\bar{h}_z)) = (0.955, 1.058), (0.920, 1.715), (0.875, 2.484)$, we obtain $\ln C = 4.27$.

The available numerical data for $\bar{\Delta}^1(\bar{h}_z)$ in the intermediate phase range $-u < h_z < u$ visually extrapolate well to the value $\bar{\Delta}^1(\bar{h}_z = -1) = 4\pi$ [Eqs. (6.15) and (6.16)] of the bulk skyrmion at the phase transition point $h_z = -u$.

The typical edge charge configuration $\mathbf{n}_0^1(\mathbf{r})$ in the $\mathbf{n}^\infty = \mathbf{n}^*(\varphi_0)$ phase is shown in Fig. 10. In Fig. 12, the angle functions $\theta_0^1(x, 0)$ and $\varphi_0^1(x = -0, y)$ of $\mathbf{n}_0^1(\mathbf{r})$ are plotted for various \bar{h}_z . The regions where these functions vary determine the size of the charge excitation. As h_z decreases in the range $-u < h_z < u$, this size monotonically decreases, becoming smaller than l_u .

These behaviors of the gap and size of the excitation with decreasing h_z in the $-u < h_z < u$ region are in accord with the general arguments of Sec. VIC that in the $\mathbf{n}^\infty = -\mathbf{n}_z$ phase at $h_z < -u$, the charge excitations are skyrmions with zero size [for the considered model with neglected Coulomb self-interaction of the charge density (6.1)].

F. Summary

To summarize, in this section, we studied the edge charge excitations. We found that the properties of the charge excitations of the phases $\mathbf{n}^\infty = \pm\mathbf{n}_z$ with preserved U(1) symmetry remain qualitatively the same in the presence of strong interactions: the TnT phase $\mathbf{n}^\infty = \mathbf{n}_z$ has gapless edge excitations and the TT phase $\mathbf{n}^\infty = -\mathbf{n}_z$ has gapped edge excitations. However, collective charge excitations of the interacting system are microscopically quite different from the single-electron excitations of the noninteracting system.

In the intermediate phase $\mathbf{n}^\infty = \mathbf{n}^*(\varphi_0)$ with spontaneously broken U(1) symmetry the edge charge excitations are gapped. This suggests that the U(1) symmetry is responsible for the topological protection in this strongly interacting system. This important point will be further substantiated in the next Sec. VII, where we study the low-energy edge dynamics of the TnT phase $\mathbf{n}^\infty = \mathbf{n}_z$, including the effects of (non-spontaneous) U(1) symmetry breaking, Secs. IIC and IIIC.

We point out here that, since rigorous mathematical definitions of topological phases in interacting systems are currently an actively researched subject, in this arti-

cle, we adopt an intuitive nomenclature, whereby we refer to the phases with gapless and gapped edge excitations as TnT and TT phases, respectively.

We also point out that while the properties of the edge excitations of the three phases are different, their bulk charge excitations are qualitatively the same: the bulk charge gap is finite in all three phases and never closes during the transformation from the TnT $\mathbf{n}^\infty = \mathbf{n}_z$ to the TT $\mathbf{n}^\infty = -\mathbf{n}_z$ phase with increasing h_z . This is another qualitative distinction from the single-particle noninteracting picture, where the topological phase transition is associated with the closing of the bulk gap.

VII. HELICAL LUTTINGER LIQUID

A. Derivation

In the previous Sec. VI, it was demonstrated that the $\mathbf{n}^\infty = \mathbf{n}_z$ phase at $u < h_z$ is characterized by gapless charge edge excitations. In this section, we derive the effective low-energy theory describing the dynamics of these edge excitations. The criterion for the applicability of such a low-energy theory is quite clear at the physical level: the nondegenerate bulk ground state $\mathbf{n}^\infty = \mathbf{n}_z$ has a gapped excitation spectrum and the theory is valid at energies below this gap $h_z - u$, i.e., as long as the bulk is not excited. This criterion will be established more rigorously below.

The gapless edge excitations originate from the degeneracy of the (mean-field) ground state solution $\mathbf{n}_0(x; \varphi_0)$ at the edge, characterized by an arbitrary angle φ_0 . Essentially, now we would like to include the slow variations of the angle φ_0 in space and time and perform a gradient expansion. Since some terms in the original Lagrangian $\mathbb{L}[\theta, \varphi]$ [Eqs. (3.3)-(3.6)] couple the $\varphi(\mathbf{r}; t)$ and $\theta(\mathbf{r}; t)$ variables, $\theta(\mathbf{r}; t)$ cannot just be considered as static and replaced by the ground state configuration $\theta_0(x)$. However, the deviations from the ground state configurations due to slowly varying $\varphi(\mathbf{r}; t)$ will be small, and so the Lagrangian $\mathbb{L}[\theta, \varphi]$ may be expanded in deviations $\delta\theta(\mathbf{r}; t)$ about $\theta_0(x)$,

$$\theta(\mathbf{r}; t) = \theta_0(x) + \delta\theta(\mathbf{r}; t). \quad (7.1)$$

The deviation must satisfy the boundary condition

$$\delta\theta(x = 0, y; t) = 0. \quad (7.2)$$

For now, we assume a general, but slow, dependence of $\varphi(\mathbf{r}, t)$ on \mathbf{r} and t ; further approximations to follow.

To the leading order in gradients of $\varphi(\mathbf{r}; t)$, it is sufficient to expand different terms to the lowest necessary order in $\delta\theta(\mathbf{r}; t)$. This way, for the kinetic term (3.4), we have

$$K[\delta\theta, \varphi] = \frac{\dot{\varphi}}{2}[\cos\theta_0 + \delta\theta\partial_\theta\cos\theta_0 + \mathcal{O}(\delta\theta^2)] \rightarrow \frac{\dot{\varphi}}{2}\delta\theta\partial_\theta\cos\theta_0. \quad (7.3)$$

The term $\frac{\dot{\varphi}}{2}\cos\theta_0$ is an inconsequential full time derivative and may be dropped. For the reason to be provided below, we keep the derivative $\partial_\theta\cos\theta_0 = -\sin\theta_0$ as is, without explicitly differentiating it.

In the gradient term

$$\frac{\rho}{2}\sin^2\theta(\nabla\varphi)^2 = \frac{\rho}{2}[\sin^2\theta_0(x) + \mathcal{O}(\delta\theta)](\nabla\varphi)^2 \rightarrow \frac{\rho}{2}\sin^2\theta_0(x)(\nabla\varphi)^2 \quad (7.4)$$

in Eq. (3.5), keeping only the zero-order term is sufficient.

The remaining terms

$$\int \frac{d^2\mathbf{r}}{s} \left\{ \frac{\rho}{2}(\nabla\theta)^2 + \mathcal{E}(\theta) \right\} = \int \frac{d^2\mathbf{r}}{s} \left\{ E[\mathbf{n}_0] + \frac{1}{2}\delta\theta\hat{U}[\delta\theta] + \mathcal{O}(\delta\theta^3) \right\} \rightarrow \int \frac{d^2\mathbf{r}}{s} \frac{1}{2}\delta\theta\hat{U}[\delta\theta] \quad (7.5)$$

in Eq. (3.5) do not depend on $\varphi(\mathbf{r}; t)$ and need to be expanded to quadratic order (the zero-order ground state energy $\mathbb{E}[\mathbf{n}_0]$ may be dropped and the linear order in $\delta\theta(\mathbf{r}; t)$ vanishes since $\theta_0(x)$ minimizes exactly this functional). Here,

$$\hat{U} = -\rho\nabla_y^2 + \hat{U}_x, \quad (7.6)$$

$$\hat{U}_x = -\rho\nabla_x^2 + \partial_\theta^2\mathcal{E}(\theta_0(x)), \quad (7.7)$$

$$\partial_\theta^2\mathcal{E}(\theta) = -u\cos 2\theta + h_z\cos\theta. \quad (7.8)$$

Collecting these leading terms [Eqs. (7.3), (7.4), and (7.5)], we approximate the initial Lagrangian as

$$\mathbb{L}[\theta, \varphi] \rightarrow \mathbb{L}'[\delta\theta, \varphi] = \int \frac{d^2\mathbf{r}}{s} L'[\delta\theta, \varphi],$$

$$-L'[\delta\theta, \varphi] \equiv -\frac{\dot{\varphi}}{2}\delta\theta\partial_\theta\cos\theta_0 + \frac{1}{2}\delta\theta\hat{U}[\delta\theta] + \frac{\rho}{2}\sin^2\theta_0(\nabla\varphi)^2. \quad (7.9)$$

The structure of the Lagrangian (7.9) allows for further approximations.

First, we observe that in both terms containing the $\varphi(\mathbf{r}; t)$ variable, the function $\sin\theta_0(x)$ is present, which constrains them to the domain-wall region of size l_u . We split the field

$$\varphi(x, y; t) = \Phi(y; t) + \delta_x\varphi(x, y; t)$$

into an x -independent average

$$\Phi(y; t) \equiv \langle \varphi(x, y; t) \rangle_x \quad (7.10)$$

along x and fluctuations $\delta_x\varphi(x, y; t)$, which are, by this construction, zero on average,

$$\langle \delta_x\varphi(x, y; t) \rangle_x = 0.$$

There is certain freedom in the definition of this average. Since the parametrization by the spherical angles becomes degenerate at $\theta = 0, \pi$, a meaningful average requires a weight function that takes that into account. The most reasonable weight function seems to be $\sin\theta_0(x)$, and so we define the average as

$$\langle f(x) \rangle_x \equiv \int_{-\infty}^0 dx \sin\theta_0(x) f(x).$$

Although other similar choices could also be used, to the leading order, when $\delta_x\varphi$ is just neglected, the exact definition of the average is not essential.

Since at low energies $\varphi(x, y; t)$ varies over spatial scales exceeding the domain wall size l_u , the fluctuations of the field $\varphi(x, y; t)$ in the x direction across the domain wall, described by $\delta_x\varphi(x, y; t)$, will produce a parametrically smaller contribution than those in the y direction along the domain wall, described by $\Phi(y; t)$. Thus, to the leading order, $\delta_x\varphi(x, y; t)$ may be neglected and the field

$$\varphi(x, y; t) \rightarrow \Phi(y; t) \quad (7.11)$$

may be approximated by a quasi-1D field $\Phi(y; t)$. After this approximation, the gradient term becomes $(\nabla\varphi)^2 \rightarrow (\nabla_y\Phi)^2$.

Next, we analyze the properties of the operator \hat{U}_x [Eq. (7.7)]. The operator \hat{U}_x has the form of the Hamiltonian for a Schrödinger particle in 1D with the potential energy $\partial_\theta^2\mathcal{E}(\theta_0(x))$ [Eq. (7.8)], plotted in Fig 13, and the “hard wall” boundary condition (7.2). In the bulk,

$$\partial_\theta^2\mathcal{E}(\theta_0(-\infty) = 0) = h_z - u > 0,$$

which represents the mass of the “isospin wave” in an infinite system. The minimum

$$\partial_\theta^2\mathcal{E}(\theta_0(0) = \pi) = -h_z - u < 0$$

is reached at the edge and is negative. The “potential energy” $\partial_\theta^2\mathcal{E}(\theta_0(x))$ curve has a “well” in the region

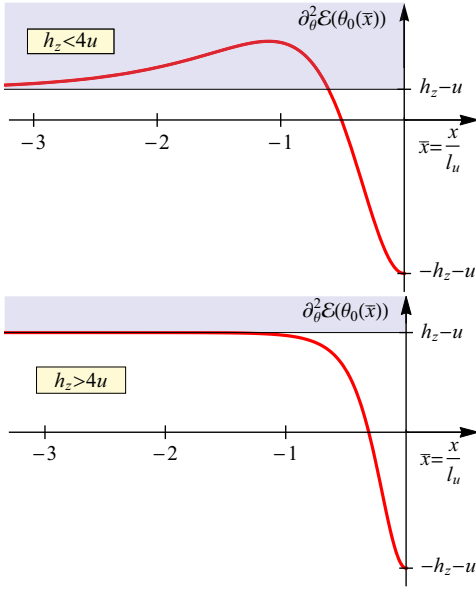


FIG. 13: The function $\partial_\theta^2 \mathcal{E}(\theta_0(x))$ [Eq. (7.8)], which serves as an effective potential in the operator \hat{U}_x [Eq. (7.7)], which describes the quadratic fluctuations $\delta\theta$ [Eq. (7.1)] about the ground state configuration $\theta_0(x)$ [Eq. (5.11)] in the $\mathbf{n}^\infty = \mathbf{n}_z$ phase at $u < h_z$. The operator \hat{U}_x has only a continuous spectrum, marked by a shaded region, that starts at the bulk asymptotic value $\partial_\theta^2 \mathcal{E}(\theta_0(x = -\infty)) = h_z - u$, equal to the gap of the bulk isospin wave excitations, and there are no discrete bound states.

of the domain wall; for $h_z < 4u$, it also has a “barrier”. From this analogy with the quantum-mechanical problem, we conclude that the operator \hat{U}_x has a continuous eigenvalue spectrum in the energy range $(h_z - u, +\infty)$, but it *could* also have discrete levels in the range $(-h_z - u, h_z - u)$, which would correspond to the “states” bound within the well. However, we have checked numerically that there are no such discrete eigenvalues. In fact, only the positive range $(0, h_z - u)$ requires a check for bound states, since negative eigenvalues are prohibited because \hat{U}_x is a quadratic form of the expansion about the minimum-energy configuration and is therefore a positive-definite operator.

Thus, \hat{U}_x has only a continuous “massive” eigenvalue

spectrum that starts from $h_z - u > 0$. The eigenfunctions are extended and can basically be viewed as bulk isospin waves somewhat modified at the edge.

Due to these properties, the operator $-\rho\nabla_y^2$ in \hat{U} [Eq. (7.6)] may be neglected compared to \hat{U}_x ,

$$\hat{U} = -\rho\nabla_y^2 + \hat{U}_x \rightarrow \hat{U}_x. \quad (7.12)$$

The approximations (7.11) and (7.12) allow us to further simplify the Lagrangian (7.9) as

$$\begin{aligned} \mathbb{L}'[\delta\theta, \varphi] &\rightarrow \mathbb{L}''[\delta\theta, \Phi] = \int \frac{d^2\mathbf{r}}{s} L''[\delta\theta, \Phi], \\ -L''[\delta\theta, \Phi] &\equiv -\frac{\dot{\Phi}}{2} \delta\theta \partial_\theta \cos \theta_0 + \frac{1}{2} \delta\theta \hat{U}_x[\delta\theta] + \frac{\rho}{2} \sin^2 \theta_0 (\nabla_y \Phi)^2. \end{aligned} \quad (7.13)$$

The Lagrangian (7.13) is a second-order functional polynomial in $\delta\theta(\mathbf{r}; t)$. Consider the configuration $\delta\theta_0[\Phi](\mathbf{r}; t)$ that delivers the minimum of $-\mathbb{L}''[\delta\theta, \Phi]$ with respect to $\delta\theta(\mathbf{r}; t)$ for a given $\Phi(y; t)$. It satisfies the stationary-point equation

$$-\frac{\delta}{\delta(\delta\theta)} \int dt \mathbb{L}''[\delta\theta, \Phi] = -\frac{\dot{\Phi}}{2} \partial_\theta \cos \theta_0 + \hat{U}_x[\delta\theta] = 0. \quad (7.14)$$

This is a differential-in- x equation, and its solution can thus be formally written as

$$\delta\theta_0[\Phi](\mathbf{r}; t) = \partial\theta_0(x) \frac{\dot{\Phi}(y; t)}{2}, \quad (7.15)$$

where

$$\partial\theta_0(x) = \hat{U}_x^{-1}[\partial_\theta \cos \theta_0]. \quad (7.16)$$

The reason for the notation $\partial\theta_0(x)$ will become clear shortly.

In terms of this minimum configuration and the deviation

$$\delta\tilde{\theta}(\mathbf{r}; t) = \delta\theta(\mathbf{r}; t) - \delta\theta_0[\Phi](\mathbf{r}; t)$$

from it, the Lagrangian (7.13) can be rewritten identically as

$$-L''[\delta\theta_0[\Phi] + \delta\tilde{\theta}, \Phi] = -\frac{1}{2} \left(\frac{\dot{\Phi}}{2} \right)^2 \partial\theta_0(x) \partial_\theta \cos \theta_0(x) + \frac{\rho}{2} \sin^2 \theta_0(x) (\nabla_y \Phi)^2 + \frac{1}{2} \delta\tilde{\theta} \hat{U}_x[\delta\tilde{\theta}]. \quad (7.17)$$

This procedure essentially amounts to completing the square of the quadratic polynomial in the functional sense. This way, decoupling of the field $\Phi(y; t)$ and the variables (“free modes”) $\delta\tilde{\theta}(\mathbf{r}; t)$ of the operator \hat{U}_x

has been achieved. Since the latter have a gap $h_z - u$, their contribution may be neglected below this energy scale. In the end, this amounts to replacing $-\mathbb{L}''[\delta\theta, \Phi]$ in Eq. (7.13) by its minimum with respect to $\delta\theta(\mathbf{r}; t)$. This

minimum is given by the first two terms in Eq. (7.17) and represents the sought effective Lagrangian:

$$\mathbb{L}^{1\text{D}}[\Phi] \equiv \mathbb{L}''[\delta\theta_0[\Phi], \Phi].$$

The y -dependent 1D field $\Phi(y; t)$ is the only remaining variable, while the rest is fixed functions of x . This allows us to separate them and write the final Lagrangian for the edge excitations of the $\mathbf{n}^\infty = \mathbf{n}_z$ phase in the form:

$$\mathbb{L}^{1\text{D}}[\Phi] = \int dy L^{1\text{D}}[\Phi], \quad L^{1\text{D}}[\Phi] = \frac{1}{2\pi\mathcal{K}} \left[\frac{1}{v} \dot{\Phi}^2 - v(\nabla_y \Phi)^2 \right]. \quad (7.18)$$

We recognize in Eq. (7.18) the Lagrangian of a Luttinger liquid, with the phase field $\Phi(y; t)$ at the edge being the collective bosonic variable. The parameters v and \mathcal{K} are given by

$$\frac{1}{2\pi\mathcal{K}v} \equiv \frac{l_u}{su} F_t(\bar{h}_z), \quad F_t(\bar{h}_z) \equiv \frac{u}{8} \int_{-\infty}^0 d\bar{x} \partial_\theta \cos \theta_0(x) \partial \theta_0(x) = \frac{u}{8} \int_{-\infty}^0 d\bar{x} \partial_\theta \cos \theta_0 \hat{U}_x^{-1}[\partial_\theta \cos \theta_0], \quad (7.19)$$

$$\frac{v}{2\pi\mathcal{K}} \equiv \frac{\rho l_u}{s} F_y(\bar{h}_z), \quad F_y(\bar{h}_z) = \frac{1}{2} \int_{-\infty}^0 d\bar{x} \sin^2 \theta_0(\bar{x}; \bar{h}_z). \quad (7.20)$$

Due to the scaling form $\theta_0(x) = \theta_0(\bar{x}; \bar{h}_z)$ of the ground state solution (5.11), the parameters can be expressed in terms of the dimensionless functions $F_{t,y}(\bar{h}_z)$ of the normalized field $\bar{h}_z = h_z/u$.

We recognize that $F_y(\bar{h}_z) = F_2(\bar{h}_z)$ [Eq. (5.23)], which is not surprising, since this quantity has already appeared in an essentially identical calculation of Eq. (6.12) in Sec. VIB. On the other hand, without additional insights, calculating $F_t(\bar{h}_z)$ would require first finding the solution $\partial\theta_0(x)$ [Eq. (7.16)] to the differential equation (7.14) and then calculating the integral in Eq. (7.19). Below we provide a more elegant and streamlined way of deriving the low-energy model (7.18), which not only allows us to obtain the explicit expression for $F_t(\bar{h}_z)$, but also uncovers the origin of the low-energy model in the degenerate ground state solution. The above derivation is nonetheless useful for justifying the employed approx-

imations.

We make two crucial observations about the general structure of the Lagrangian (3.3)-(3.6).

First, we observe that the kinetic term $\frac{\dot{\varphi}}{2} \cos \theta$ [Eq. (3.4)] has the same structure as the "Zeeman" term $-h_z \cos \theta$ in Eqs. (3.5) and (3.6), in which $\frac{\dot{\varphi}}{2}$ plays the role of an additional (in general, time- and coordinate-dependent) "Zeeman" field.

Second, as already noticed in Sec. VIB, we observe that the gradient term $\frac{\rho}{2} \sin^2 \theta (\nabla \varphi)^2$ has the form of the anisotropy $\frac{u}{2}(n_z^2 - 1)$, in which $-\rho(\nabla \varphi)^2$ plays the role of an additional anisotropy energy.

These two observations allow us to rewrite the Lagrangian density (3.3) identically as [Eqs. (5.18) and (5.19)]

$$-L[\theta, \varphi; u, h_z] = E[\theta, \varphi; u, h_z + \frac{\dot{\varphi}}{2}] = dE_x[\theta; u - \rho(\nabla \varphi)^2, h_z + \frac{\dot{\varphi}}{2}] + \frac{\rho}{2} (\nabla_y \theta)^2 + \mathcal{E}^\infty(u, h_z)$$

After the two key approximations, (i) considering only- y -dependent configurations $\varphi(\mathbf{r}; t) \rightarrow \Phi(y; t)$ [Eq. (7.11)] and (ii) neglecting the gradient terms $\nabla_y \theta$ [Eq. (7.12)], the Lagrangian density per unit length in the y direction

$$-\int \frac{dx}{s} L[\theta, \varphi; u, h_z] \rightarrow dE^{1\text{D}}[\theta; u - \rho(\nabla_y \Phi)^2, h_z + \frac{\dot{\Phi}}{2}] + E^{1\text{D}\infty}(u, h_z) \quad (7.21)$$

becomes equivalent to the functional (5.6) for the ground state with the modified parameters. The functional (7.21) is minimized by the modified ground state configuration $\theta_0(x; u - \rho(\nabla_y \Phi)^2, h_z + \frac{\dot{\Phi}}{2})$ [Eq. (5.11)] and the minimum

$$-\tilde{L}^{1\text{D}}[\Phi] = dE_0^{1\text{D}} \left(u - \rho(\nabla_y \Phi)^2, h_z + \frac{\dot{\Phi}}{2} \right) - dE^{1\text{D}}(u, h_z) \quad (7.22)$$

is expressed in terms of the domain wall energy (5.21). Its expansion up to the quadratic order in the derivatives yields the form

$$-\tilde{L}^{1D}[\Phi] \approx -\partial_u dE_0^{1D}(u, h_z) \rho(\nabla_y \Phi)^2 + \partial_{h_z} dE_0^{1D}(u, h_z) \frac{\dot{\Phi}}{2} + \frac{1}{2} \partial_{h_z}^2 dE_0^{1D}(u, h_z) \left(\frac{\dot{\Phi}}{2} \right)^2 = -L^{1D}[\Phi] + \partial_{h_z} dE_0^{1D}(u, h_z) \frac{\dot{\Phi}}{2} \quad (7.23)$$

of the Luttinger liquid Lagrangian (7.18). As in Eq. (7.3), the term linear in $\dot{\Phi}$ is an inconsequential full time derivative and may be dropped. This allows us to express the parameters

$$\frac{1}{2\pi\mathcal{K}v} = -\frac{1}{8} \partial_{h_z}^2 dE_0^{1D}(u, h_z), \quad \frac{v}{2\pi\mathcal{K}} = -\rho \partial_u dE_0^{1D}(u, h_z)$$

of the Luttinger liquid in terms of the derivatives of the domain-wall energy and thus calculate the coefficients $F_{t,y}$ [Eqs. (7.19) and (7.20)] explicitly as

$$F_t(\bar{h}_z) = -\frac{1}{4} \partial_{\bar{h}_z}^2 F(\bar{h}_z) = \frac{1}{8} \frac{1}{\bar{h}_z \sqrt{\bar{h}_z - 1}}, \quad (7.24)$$

$$F_y(\bar{h}_z) = F_2(\bar{h}_z) = \bar{h}_z \arcsin \frac{1}{\sqrt{\bar{h}_z}} - \sqrt{\bar{h}_z - 1} \quad (7.25)$$

The functions are plotted in Fig. 14. Their asymptotic expressions at the transition point and at large h_z are

$$F_t(\bar{h}_z) = \frac{1}{8} \begin{cases} \frac{1}{\sqrt{\bar{h}_z - 1}}, & h_z \rightarrow u + 0, \\ \frac{1}{\bar{h}_z^{3/2}}, & h_z \gg u, \end{cases} \quad (7.26)$$

$$F_y(\bar{h}_z) = \begin{cases} \frac{\pi}{2}, & h_z \rightarrow u + 0, \\ \frac{2}{3} \frac{1}{\sqrt{\bar{h}_z}}, & h_z \gg u. \end{cases} \quad (7.27)$$

Also, according to this approach, the function $\delta\theta_0[\Phi](\mathbf{r}; t)$ [Eqs. (7.15) and (7.16)] can be identified as the linear term of the expansion of $\theta_0(x; u, h_z + \frac{\dot{\Phi}}{2})$ in $\frac{\dot{\Phi}}{2}$. Therefore, the function (7.16)

$$\partial\theta_0(x) = \partial_{h_z} \theta_0(x; u, h_z) \quad (7.28)$$

is the derivative of the ground state solution with respect to h_z . Inserting this form into Eq. (7.19) for $F_t(\bar{h}_z)$, we then observe that the integrand is a full derivative with respect to h_z (which is the reason for not differentiating $\partial_\theta \cos \theta_0$ explicitly), and the coefficient can alternatively be expressed in terms of $F_1(\bar{h}_z)$ [Eq. (5.24)] as

$$F_t(\bar{h}_z) = \frac{1}{8} \int_{-\infty}^0 d\bar{x} \partial_{\bar{h}_z} \cos \theta_0(\bar{x}; \bar{h}_z) = -\frac{1}{4} \partial_{\bar{h}_z} F_1(\bar{h}_z), \quad (7.29)$$

which, of course, agrees with (7.24).

This method of the derivation of the Luttinger liquid model (7.18) as an expansion of the modified domain-wall energy also allows us to determine the restrictions on the allowed magnitude of fluctuations. The domain-wall energy $dE_0^{1D}(u, h_z)$ [Eq. (5.21)] contains a nonanalytic square-root dependence $\sqrt{\bar{h}_z - 1}$. As a result, the

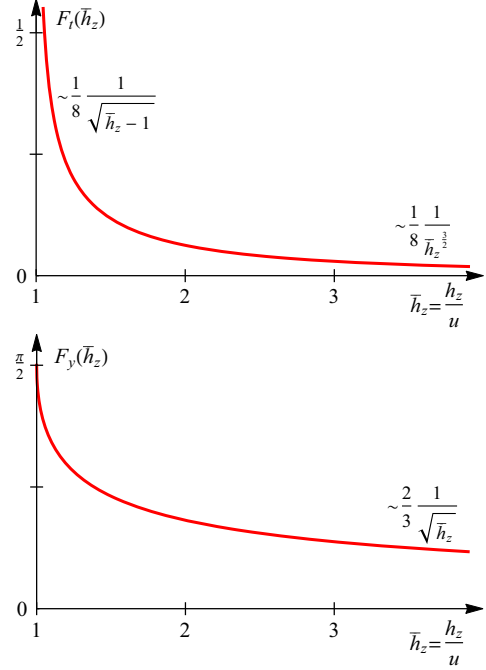


FIG. 14: (Color online) The functions $F_t(\bar{h}_z)$ [Eq. (7.19)] and $F_y(\bar{h}_z)$ [Eq. (7.20)] that determine the coefficients in front of the time- and coordinate-derivative terms in the Luttinger liquid model (7.18) for the edge excitations of the TnT $\mathbf{n}^\infty = \mathbf{n}_z$ phase. The asymptotic functions (7.26) and (7.27) at the transition point $\bar{h}_z = 1$ and at large $\bar{h}_z \gg 1$ are indicated.

power expansion (7.23) is valid as long as the fluctuation energies

$$\dot{\Phi}, \rho(\nabla_y \Phi)^2 \ll h_z - u \quad (7.30)$$

are much smaller than the deviation $h_z - u$ from the transition point. This deviation, as one would expect, coincides with the gap of the neutral bulk excitations (isospin waves).

In this regard, we caution about using the unexpanded functional (7.22) at fluctuation energies $\dot{\Phi}$ and $\rho(\nabla_y \Phi)^2$ comparable to $h_z - u$: while this is an essentially exact expression *under the made approximations*, these approximations amount to neglecting other isospin configurations, such as bulk excitations, which become relevant at energies $\sim h_z - u$.

In the next Sec. VII B, we analyze the main properties of the obtained Luttinger liquid model.

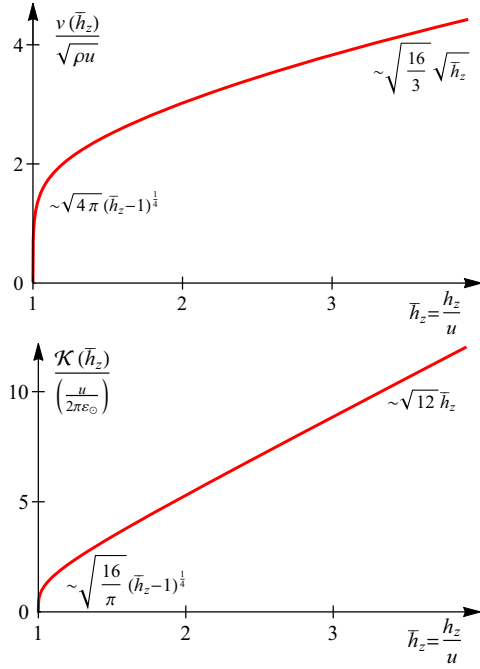


FIG. 15: (Color online) The velocity $v(\bar{h}_z)$ [Eq. (7.33)] and interaction parameter $\mathcal{K}(\bar{h}_z)$ [Eq. (7.34)] of the Luttinger liquid model (7.18) for the edge excitations of the TnT $\mathbf{n}^\infty = \mathbf{n}_z$ phase. The asymptotic functions (7.35) and (7.36) at the transition point $\bar{h}_z = 1$ and at large $\bar{h}_z \gg 1$ are indicated.

B. Analysis

The Luttinger liquid model (7.18) describes the edge excitations of the $\mathbf{n}^\infty = \mathbf{n}_z$ phase, realized at $u < h_z$; its collective variable is the angle $\Phi(y; t)$ varying with time t and coordinate y along the edge. To the leading approximation, the isospin texture associated with $\Phi(y; t)$ is given by the “deformed” ground state configuration $\mathbf{n}_0(x|\Phi(y; t))$ [Eqs. (5.5) and (5.11)]. The field $\Phi(y; t)$ thus corresponds to polarization in the xy isospin plane.

Simultaneously, this edge isospin texture carries electric charge. According to Eq. (6.1), the charge density per unit length in the y direction, integrated over a cross-section of constant y , reads

$$\begin{aligned} \kappa^{1D}[\Phi](y; t) &\equiv \int_{-\infty}^0 dx \kappa[\mathbf{n}_0(x|\Phi(y; t))] \\ &= \frac{1}{4\pi} \int_{-\infty}^0 dx \sin \theta_0(x) \nabla_x \theta_0(x) \nabla_y \Phi(y; t) \\ &= \frac{1}{2\pi} \nabla_y \Phi(y; t). \end{aligned} \quad (7.31)$$

The associated electric current in the y direction equals

$$j^{1D}[\Phi](y; t) = -\frac{1}{2\pi} \dot{\Phi}(y; t), \quad (7.32)$$

as follows from the continuity equation

$$\dot{\kappa}^{1D} + \nabla_y j^{1D} = 0.$$

Therefore, the single field $\Phi(y; t)$ carries both isospin and charge degrees of freedom, “locked” to each other, and the Luttinger liquid (7.18) represents an isospin “helical” liquid¹⁶.

The theory is fully characterized by two parameters: the velocity v of the linear gapless excitation spectrum $\omega = vk$ and the dimensionless parameter \mathcal{K} describing the effective strength of interactions³¹. We remind the reader that in a generic Luttinger liquid $\mathcal{K} = 1$ corresponds to a noninteracting system; $0 < \mathcal{K} < 1$ is the range of repulsive interactions, the stronger the interactions, the smaller \mathcal{K} ; and $1 < \mathcal{K}$ is the range of attractive interactions, the stronger the interactions, the larger \mathcal{K} .

From Eqs. (7.19) and (7.20), the parameters are expressed in terms of the functions $F_{t,y}(\bar{h}_z)$ [Eqs. (7.24) and (7.25)] as

$$v(\bar{h}_z) = \sqrt{\rho u} \sqrt{\frac{F_y(\bar{h}_z)}{F_t(\bar{h}_z)}}, \quad (7.33)$$

$$\mathcal{K}(\bar{h}_z) = \frac{u}{2\pi\epsilon_\odot} \frac{1}{\sqrt{F_t(\bar{h}_z)F_y(\bar{h}_z)}}. \quad (7.34)$$

Their asymptotic expressions at the phase transition point $h_z = u$ and at large h_z , following Eqs. (7.26) and (7.27), are

$$v(\bar{h}_z) = \sqrt{\rho u} \begin{cases} \sqrt{4\pi}(\bar{h}_z - 1)^{\frac{1}{4}}, & h_z \rightarrow u + 0, \\ \sqrt{\frac{16}{3}}\sqrt{\bar{h}_z}, & h_z \gg u. \end{cases} \quad (7.35)$$

$$\mathcal{K}(\bar{h}_z) = \frac{u}{2\pi\epsilon_\odot} \begin{cases} \sqrt{\frac{16}{\pi}}(\bar{h}_z - 1)^{\frac{1}{4}}, & h_z \rightarrow u + 0, \\ \sqrt{12}\bar{h}_z, & h_z \gg u. \end{cases} \quad (7.36)$$

The dependence of the parameters $v(\bar{h}_z)$ and $\mathcal{K}(\bar{h}_z)$ on the normalized field \bar{h}_z is plotted in Fig. 15 and follows from the behavior of the functions $F_y(\bar{h}_z)$ and $F_t(\bar{h}_z)$, plotted in Fig. 14.

Both the velocity $v(\bar{h}_z)$ and interaction parameter $\mathcal{K}(\bar{h}_z)$ are growing functions of the field \bar{h}_z i.e., increase as the magnetic field B decreases. Not too close to the phase transition $h_z = u$, when $h_z - u \gtrsim u$, they scale as

$$v \sim \sqrt{\rho \max\{u, h_z\}} \sim e_*^2 \sqrt{\frac{\max\{u, h_z\}}{\epsilon_\odot}}, \quad (7.37)$$

$$\mathcal{K} \sim \frac{\max\{u, h_z\}}{\epsilon_\odot} \ll 1. \quad (7.38)$$

Thus, in the whole range of applicability of the QHFM theory, when the energy scales $u, h_z \ll \epsilon_\odot$ of the SU(2)-asymmetric terms are much smaller than that ϵ_\odot of the SU(2)-symmetric interactions, set by the Coulomb energy [Eq. (6.13)], the interaction parameter $\mathcal{K} \ll 1$ is small and the Luttinger liquid is *strongly interacting*.

Moreover, since $F_t(\bar{h}_z \rightarrow 1 + 0) \sim \frac{1}{\sqrt{\bar{h}_z - 1}}$ diverges while $F_y(\bar{h}_z = 1) = \frac{\pi}{2}$ becomes constant, both the velocity $v \sim \sqrt{\rho u}(\bar{h}_z - 1)^{\frac{1}{4}}$ and the interaction parameter $\mathcal{K} \sim \frac{u}{\epsilon_\odot}(\bar{h}_z - 1)^{\frac{1}{4}}$ approach zero at the transition

point, $h_z \rightarrow u + 0$. The Luttinger liquid therefore becomes *infinitely* strongly interacting at the transition point. We note though that the energy window of applicability of this low-energy theory narrows accordingly, see Eq. (7.30); for larger fluctuations, the Luttinger liquid model becomes invalid.

The Luttinger liquid models for the edge excitations in the form of Eq. (7.18) were obtained in Ref. 36 for the double-layer system with inverted band structure and in Ref. 29 for the F phase of the $\nu = 0$ state in graphene. However, in Ref. 36, the expression for the coefficient $F_t(\bar{h}_z)$ at the time-derivative term does not diverge at the phase transition $h_z \rightarrow u + 0$. This divergence is physical and to be expected, since the 1D model should fail at the phase transition, where the bulk modes become gapless. In Ref. 29, only the scaling of the parameters $F_{t,y}(\bar{h}_z)$, $v(\bar{h}_z)$, $\mathcal{K}(\bar{h}_z)$ at the phase transition $h_z \rightarrow u + 0$ was determined, which does agree with our asymptotic results, whereas we obtain explicit analytical expressions (7.19), (7.20), (7.33), and (7.34) for them at all $u < h_z$.

The helical Luttinger liquid model for the edge excitations above was derived in a controlled way in the QHFM regime, realized in the vicinity of the topological phase transition at $B = B^*$. However, the single-particle TnT phase is realized in the whole range $0 \leq B < B^*$ of magnetic fields. It is safe to argue that if, in the presence of interactions, the Luttinger liquid persists in the region of strong effective interactions near the transition point, it also persists at all magnetic fields down to zero, i.e., in the range $0 \leq B < B^* - \delta B_u$.

Consider the “bare” velocity $v_0(B)$ of the counter-propagating single-particle edge states at the crossing point of their energy curves, $\epsilon(p) = h_z$. It is largest at zero field $B = 0$ and monotonically decreases down to zero $v_0(B \rightarrow B^* - 0) = 0$ at the single-particle phase transition point, as shown schematically in Fig. 16. The effective strength of the interactions *at the edge* can be characterized by the dimensionless parameter $e_*^2/v_0(B)$, which is also roughly equivalent (for a “sharp enough” edge) to the ratio ε_\circ/h_z characterizing the strength of interactions *in the bulk*. The effective strengths of interactions in the bulk and at the edge are thus in accord with each other.

We remind that we work under the assumption of weak bare Coulomb interactions, Sec. II A, which can also be formulated as $v_0(B = 0) \gg e_*^2$. Thus, at zero or small fields $B \ll B^*$, the edge states are weakly interacting and the corresponding low-energy theory can be derived using the standard procedure³¹ based on the linearization of the spectrum and will have the form of a Luttinger liquid. The velocity $v(B = 0) \approx v_0(B = 0)$ of the collective excitations of this Luttinger liquid will be close to the bare velocity and the interaction parameter $\mathcal{K} \approx 1$ will be close to unity, corresponding to weak effective interactions.

On the other hand, in the QHFM regime, as we have shown above, the effective interactions in the Luttinger liquid are strong, with $v(B) \ll e_*^2$ and $\mathcal{K}(B) \ll 1$

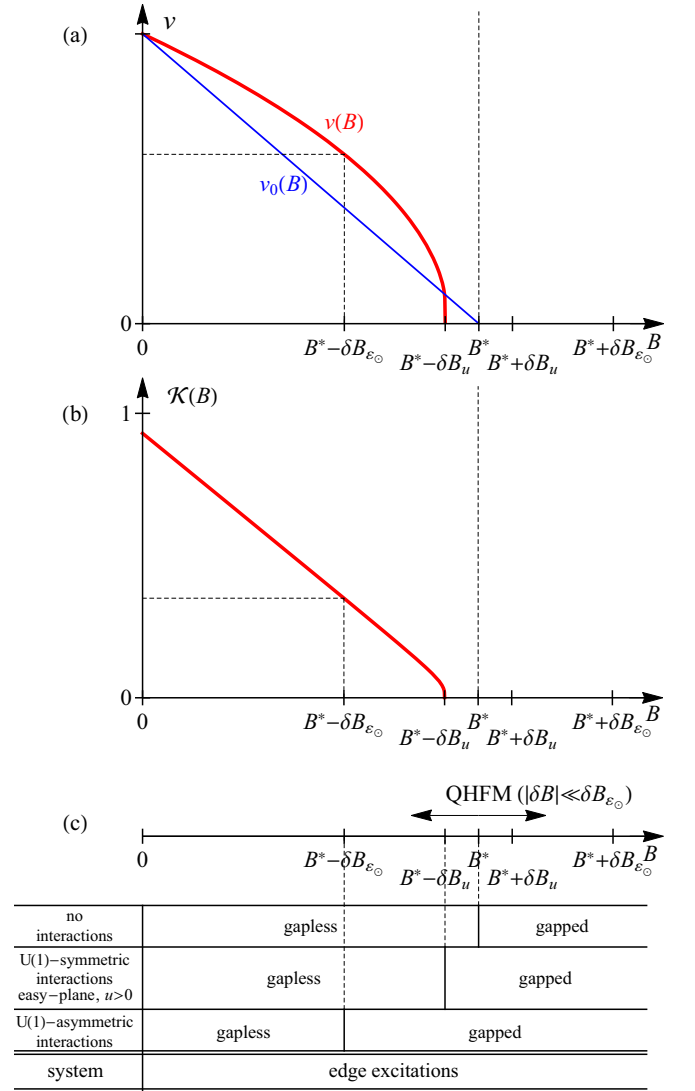


FIG. 16: (Color online) Schematic plots of the magnetic-field dependencies of the velocity $v(B)$ (a) and interaction parameters $\mathcal{K}(B)$ (b) of the helical Luttinger liquid describing the edge excitations of the TnT phase of a QHTI for U(1)-symmetric interactions with easy-plane anisotropy $u > 0$. At small fields $B \ll B^*$, the effective interactions are weak, $\mathcal{K}(B) \approx 1$, and the velocity $v(B) \approx v_0(B)$ is close to its bare value. In the QHFM regime close to the single-particle topological phase transition, the effective interactions are strong, $\mathcal{K}(B) \ll 1$. The effective interactions are thus highly tunable. (c) Summarized properties of the edge excitations. The TT phase with gapped edge excitations ensues at lower magnetic fields with switching on the interactions and lowering their symmetry.

[Eqs. (7.37) and (7.38)]. The regime of intermediate effective interaction strength with $v \sim e_*^2$ and $\mathcal{K} \sim 1$ occurs at the verge of the QHFM regime, at such fields $B = B^* - \delta B_{\varepsilon_\circ}$,

$$\delta B_{\varepsilon_\circ} \equiv \frac{\varepsilon_\circ}{|\partial_B h_z(B^*)|}, \quad (7.39)$$

where $h_z(B) \sim \varepsilon_\odot(B)$. In this intermediate-strength regime, the weakly and strongly interacting Luttinger liquids must continuously connect.

Thus, the helical Luttinger liquid describing the edge excitations of a QHTI persists in almost the whole range of the noninteracting TnT phase, $0 \leq B < B^* - \delta B_u$, and is highly tunable there: the magnetic field allows one to tune the effective interactions between weak at lower B and infinitely strong at higher B , close to the topological transition to the intermediate phase $\mathbf{n}^\infty = \mathbf{n}^*(\varphi_0)$ at $B = B^* - \delta B_u$. The corresponding behavior of the velocities $v(B)$ and interaction parameter $\mathcal{K}(B)$ in the whole range is plotted schematically in Fig. 16.

However, we remind that the derived Luttinger liquid theory for the edge was obtained under the specific assumption of U(1) isospin symmetry [Eqs. (2.10) and (2.11)] of the many-body Hamiltonian \hat{H} [Eq. (2.4)]. This U(1) symmetry is inherited by the Lagrangian (7.18) of the Luttinger liquid, which is invariant under rotations of the angle field:

$$\Phi(y; t) \rightarrow \Phi(y; t) + \phi.$$

We now turn to the analysis of the effects that break U(1) symmetry, Secs. II C and III C.

C. Broken U(1) symmetry

1. Broken physical symmetry, single-particle effect

As explained in Sec. II C, there are two categories of U(1)-asymmetric terms: ones that break the physical symmetry and exist already at the single-particle level, $\mathcal{E}_{1\varnothing}(\mathbf{n})$ [Eq. (3.9)], and the ones that preserve the physical symmetry and can arise only from interactions, $\mathcal{E}_{2\varnothing}(\mathbf{n})$ [Eq. (3.10)]. If small, these terms can be incorporated into the Luttinger liquid model (7.18).

Proceeding along the same lines as in Sec. VII, we expand the term

$$\begin{aligned} \mathcal{E}_{1\varnothing}(\mathbf{n}) &= -h_\perp [\sin \theta_0(x) + \mathcal{O}(\delta\theta)] \cos(\varphi - \varphi_{1\varnothing}) \\ &\rightarrow -h_\perp \sin \theta_0(x) \cos(\varphi - \varphi_{1\varnothing}) \end{aligned}$$

of the first category about the ground state [Eq. (7.1)] and keep only the zero-order term in $\delta\theta$. Due to the constraining function $\sin \theta_0(x)$, the approximation (7.11) for the variable $\varphi(\mathbf{r}; t)$ may then be used. This yields the contribution

$$-\mathbb{L}_{1\varnothing}^{\text{1D}}[\Phi] = -h_\perp^{\text{1D}} \int dy \cos(\Phi(y; t) - \varphi_{1\varnothing}), \quad (7.40)$$

to the 1D Lagrangian of the edge excitations, where

$$\begin{aligned} h_\perp^{\text{1D}} &= \frac{h_\perp l_u}{s} F_\perp(\bar{h}_z), \\ F_\perp(\bar{h}_z) &= \int_{-\infty}^0 d\bar{x} \sin \theta_0(\bar{x}; \bar{h}_z) = \ln \frac{\sqrt{\bar{h}_z} + 1}{\sqrt{\bar{h}_z} - 1} \end{aligned} \quad (7.41)$$

The Lagrangian $\mathbb{L}^{\text{1D}}[\Phi] + \mathbb{L}_{1\varnothing}^{\text{1D}}[\Phi]$ describes the sine-Gordon model³¹, the properties of which are well-studied. Its excitation spectrum is gapped at $\mathcal{K} < 2$, i.e., including all repulsive interactions, $0 < \mathcal{K} < 1$, the noninteracting case $\mathcal{K} = 1$, and an (irrelevant for the considered system) range $1 < \mathcal{K} < 2$ of attractive interactions.

Thus, as expected, if the physical symmetry is broken, there is no topological protection already at the single-particle level ($\mathcal{K} = 1$). As a result, in the presence of repulsive interactions ($\mathcal{K} < 1$), the system is in a TT phase with broken U(1) symmetry and gapped edge excitations for all magnetic fields $B \geq 0$.

2. Preserved physical, but broken U(1) symmetry, interaction effect

Similarly, expanding the term of the second category about the ground state, and keeping only the zeroth-order term in $\delta\theta$,

$$\begin{aligned} \mathcal{E}_{2\varnothing}(\mathbf{n}) &= \frac{1}{2} u_{2\varnothing} [\sin^2 \theta_0(x) + \mathcal{O}(\delta\theta)] \cos 2(\varphi - \varphi_{2\varnothing}) \\ &\rightarrow \frac{1}{2} u_{2\varnothing} \sin^2 \theta_0(x) \cos 2(\varphi - \varphi_{2\varnothing}), \end{aligned}$$

and performing the substitution (7.11), we obtain a contribution

$$-\mathbb{L}_{2\varnothing}^{\text{1D}}[\Phi] = u_{2\varnothing}^{\text{1D}} \int dy \cos 2(\Phi(y; t) - \varphi_{2\varnothing}) \quad (7.42)$$

to the 1D Lagrangian of the edge excitations, where

$$u_{2\varnothing}^{\text{1D}} = \frac{u_{2\varnothing} l_u}{s} F_y(\bar{h}_z).$$

Note that the coefficient $u_{2\varnothing}^{\text{1D}}$ appears to be given by the same function $F_y(\bar{h}_z)$ [Eq. (7.20)] as for the gradient term.

Therefore, for preserved physical symmetry (inversion), the edge is described by the Lagrangian $\mathbb{L}^{\text{1D}}[\Phi] + \mathbb{L}_{2\varnothing}^{\text{1D}}[\Phi]$. This is also a sine-Gordon model, but Eq. (7.42) differs from Eq. (7.40) by the numerical factor (2 instead of 1) in the cosine argument. As a result, the edge ground state breaks U(1) symmetry (the field acquires a finite expectation value $\langle \Phi \rangle \neq 0$) and the edge excitations become gapped in a different range of interaction strength, namely at $\mathcal{K} < \frac{1}{2}$. According to Sec. VII B, the quantum phase transition at the field $B_{2\varnothing} \sim B^* - \delta B_{\varepsilon_\odot}$ [Eq. (7.39)] such that $\mathcal{K}(B_{2\varnothing}) = \frac{1}{2}$ occurs at the verge of the QHFM regime, where $h_z(B_{2\varnothing}) \sim \varepsilon_\odot(B_{2\varnothing})$. The system has gapless edge excitations for lower fields $B < B_{2\varnothing}$ and gapped excitations for all higher fields $B > B_{2\varnothing}$.

VIII. ROLE OF U(1) SYMMETRY FOR TOPOLOGICAL PROTECTION

One of the key questions raised in the studies of topological systems is how interactions affect the topological

properties. A common understanding is that a noninteracting topological insulator is generally not guaranteed to remain such in the presence of interactions. Our present findings allow us to specify the symmetry requirements for the topological protection in the presence of interactions.

We remind that the QHTIs we consider are protected by some physical symmetry, see Sec. IA. Due to this symmetry, two relevant LLs (Fig. 1) have different transformation properties and are thus not coupled at the single-particle level. As a result, the projected *single-particle* Hamiltonian within these two LLs possesses U(1) symmetry with respect to uniaxial isospin rotations [Eqs. (1.3) and (2.11)].

Aggregating the results of Secs. VI and VII, we conclude that this *effective continuous* U(1) symmetry is the one responsible for the topological protection *in the presence of interactions* in (at least) this class of systems, QHTIs. If U(1) symmetry is preserved, the TnT phase with gapless edge charge excitations persists for any effective strength of interactions, even in the QHFM regime of strong interactions, realized in the vicinity of the single-particle topological phase transition.

However, we find that the physical symmetry alone is generally not sufficient to protect the TnT phase in the presence of interactions. The interactions preserving the physical symmetry can still break U(1) symmetry and thereby destroy the TnT phase for strong enough effective interactions.

More precisely, “preserved U(1) symmetry” means that *both* (i) the bulk ground state and (ii) the interacting projected Hamiltonian are U(1)-symmetric. Accordingly, the two mechanisms by which U(1) symmetry can be broken correspond to violation of one of these conditions:

(1) First, as demonstrated in Sec. IV, even the U(1)-symmetric interactions (condition (ii) satisfied) with the right properties (“easy-plane” anisotropy) can result in a bulk ground state with spontaneously broken U(1) symmetry (condition (i) violated): the $\mathbf{n}^\infty = \mathbf{n}_0^*(\varphi_0)$ phase. As demonstrated in Sec. VI, this phase has gapped edge charge excitations and is thus TT.

(2) Second, as demonstrated in Secs. IIC and IIIC, interactions can (depending on the physical symmetry) contain terms that preserve the physical symmetry, but break the effective U(1) symmetry (condition (ii) violated). As then shown in Sec. VIIC, these terms result in a phase transition to the TT phase with broken U(1) symmetry at the edge and gapped excitation spectrum. At the same time, the U(1)-symmetric bulk ground state $\mathbf{n}^\infty = \mathbf{n}_z$ may still persist beyond this transition (condition (i) satisfied). We mention that similar types of interactions have earlier been considered¹⁶ in the studies of helical Luttinger liquids for the edge of 2D topological insulators protected by time-reversal symmetry.

The transitions from the TnT phase to either of these TT phases occur upon increasing the magnetic field B , as the single-particle phase transition point B^* is ap-

proached and the effective interactions get stronger, but at fields *lower* than B^* : at $B^* - \delta B_u$ [Eq. (4.10)] and $B_{2\emptyset} \sim B^* - \delta B_{\varepsilon_\odot}$ [Eq. (7.39)], respectively, as summarized in Fig. 16(c). Thus, these are *interaction-induced topological quantum phase transitions*, enabled due to the tunability of the effective interactions by the magnetic field, Sec. VII B.

IX. CONCLUSION

In this work, we studied the effect of electron interactions on the topological properties of *quantum Hall topological insulators*. Due to the crossing of Landau levels at the single-particle topological phase transition, its vicinity is automatically the regime of strong effective interactions. An appealing theoretical aspect of such a system is that it can be studied in a controlled way within the framework of quantum Hall ferromagnetism.

A particular attention was paid to establishing the requirements for the topological protection in this interacting system. We find that this question is ultimately related to the effective symmetry of the system: the continuous U(1) symmetry is a necessary condition for the topologically nontrivial phase to persist in the regime of strong effective interactions.

If U(1) symmetry is preserved, the edge of the topologically nontrivial phase is described by the helical Luttinger liquid. The effective interactions of this Luttinger liquid are highly tunable by the magnetic field B : they are weak (for weak bare Coulomb interactions) at small B and grow as B is increased, becoming strong in the quantum Hall ferromagnet regime in the vicinity of the single-particle topological phase transition.

The U(1) symmetry may be broken, however, either spontaneously or by the interactions that are explicitly U(1)-asymmetric. In either scenario, this eventually results in a phase transition to a topologically trivial phase with gapped edge excitations, which can be achieved by tuning the interaction strength by the magnetic field.

The tunability of interactions, the accessibility of the regime of strong effective interactions even in a system with weak bare interactions, and the possibility to realize interaction-induced topological phase transitions are among the properties that make quantum Hall topological insulators an attractive class of systems for investigating the interplay of interactions and topology, both theoretically and experimentally.

X. ACKNOWLEDGEMENTS

We acknowledge financial support by the DFG (SPP 1666 and SFB 1170 “ToCoTronics”), the Helmholtz Foundation (VITI), and the ENB Graduate school on “Topological Insulators”.

- ¹ C.L. Kane and E.J. Mele, Phys. Rev. Lett. **95**, 146802 (2005); Phys. Rev. Lett. **95**, 226801 (2005).
- ² B. A. Bernevig, T. L. Hughes, and S.-C. Zhang, Science **314**, 1757 (2006).
- ³ M. König, S. Wiedmann, C. Brüne, A. Roth, H. Buhmann, L. W. Molenkamp, X.-L. Qi, and S.-C. Zhang, Science **318**, 766 (2007).
- ⁴ D. Hsieh, D. Qian, L. Wray, Y. Xia, Y. S. Hor, R. J. Cava, and M. Z. Hasan, Nature **452**, 970 (2008).
- ⁵ Y. Xia, D. Qian, D. Hsieh, L. Wray, A. Pal, H. Lin, A. Bansil, D. Grauer, Y. S. Hor, R. J. Cava, and M. Z. Hasan, Nat. Phys. **5**, 398 (2009).
- ⁶ I. Knez, R.-R. Du, and G. Sullivan, Phys. Rev. Lett. **107**, 136603 (2011).
- ⁷ T. Li, P. Wang, H. Fu, L. Du, K. A. Schreiber, X. Mu, X. Liu, G. Sullivan, G. A. Csáthy, X. Lin, and R.-R. Du, Phys. Rev. Lett. **115**, 136804 (2015).
- ⁸ M.Z. Hasan and C.L. Kane, Rev. Mod. Phys. **82**, 3045 (2010).
- ⁹ X.-L. Qi and S.-C. Zhang, Rev. Mod. Phys. **83**, 1057 (2011).
- ¹⁰ D. Pesin and L. Balents, Nature Physics **6**, 376 (2010).
- ¹¹ M. Dzero, K. Sun, V. Galitski, and P. Coleman, Phys. Rev. Lett. **104**, 106408 (2010)
- ¹² M. Dzero, J. Xia, V. Galitski, and P. Coleman, preprint arXiv:1506.05635 (2015).
- ¹³ Y. Lemonik, I. L. Aleiner, and V. I. Fal'ko, Phys. Rev. B **85**, 245451 (2012).
- ¹⁴ V. Cvetkovic, R. E. Throckmorton, and O. Vafek, Phys. Rev. B **86**, 075467 (2012).
- ¹⁵ A. Amaricci, J. C. Budich, M. Capone, B. Trauzettel, and G. Sangiovanni, Phys. Rev. Lett. **114**, 185701 (2015).
- ¹⁶ C. Xu and J.E. Moore, Phys. Rev. B **73**, 045322 (2006); C. Wu, B. A. Bernevig, and S.-C. Zhang, Phys. Rev. Lett. **96**, 106401 (2006); A. Ström, H. Johannesson, and G. I. Japaridze, Phys. Rev. Lett. **104**, 256804 (2010); T. L. Schmidt, S. Rachel, F. von Oppen, and L. I. Glazman, Phys. Rev. Lett. **108**, 156402 (2012); J. C. Budich, F. Dolcini, P. Recher, and B. Trauzettel, Phys. Rev. Lett. **108**, 086602 (2012); F. Crepin, J. C. Budich, F. Dolcini, P. Recher, and B. Trauzettel, Phys. Rev. B **86**, 121106(R) (2012); N. Lezmy, Y. Oreg, and M. Berkooz, Phys. Rev. B **85**, 235304 (2012); F. Geissler, F. Crepin, and B. Trauzettel Phys. Rev. B **89**, 235136 (2014); N. Kainaris, I. V. Gornyi, S. T. Carr, and A. D. Mirlin, Phys. Rev. B **90**, 075118 (2014).
- ¹⁷ M. Hohenadler and F. F. Assaad, J. Phys. Cond. Mat. **25**, 143201 (2013).
- ¹⁸ B. Scharf, A. Matos-Abiague, J. Fabian, Phys. Rev. B **86**, 075418 (2012).
- ¹⁹ D. A. Abanin, P. A. Lee, and L. S. Levitov, Phys. Rev. Lett. **96**, 176803 (2006).
- ²⁰ A. F. Young, J. D. Sanchez-Yamagishi, B. Hunt, S. H. Choi, K. Watanabe, T. Taniguchi, R. C. Ashoori, and P. Jarillo-Herrero, Nature **505**, 528 (2014).
- ²¹ Chen Fang, Matthew J. Gilbert, and B. A. Bernevig, Phys. Rev. B **86**, 115112 (2012).
- ²² K. Shiozaki and M. Sato, Phys. Rev. B **90**, 165114 (2014).
- ²³ Y.-M. Lu and D.-H. Lee, arXiv:1403.5558 (2014).
- ²⁴ C.-K. Chiu, J. C. Y. Teo, A. P. Schnyder, and S. Ryu, arXiv:1505.03535 (2015).
- ²⁵ K. Yang, K. Moon, L. Zheng, A. H. MacDonald, S. M. Girvin, D. Yoshioka, and S.-C. Zhang, Phys. Rev. Lett. **72**, 732 (1994); K. Moon, H. Mori, K. Yang, S. M. Girvin, A. H. MacDonald, L. Zheng, D. Yoshioka, and S.-C. Zhang, Phys. Rev. B **51**, 5138 (1995); K. Yang, K. Moon, L. Belkhir, H. Mori, S. M. Girvin, A. H. MacDonald, L. Zheng, and D. Yoshioka, Phys. Rev. B **54**, 11644 (1996); D. P. Arovas, A. Karlhede and D. Lilliehook, Phys. Rev. B **59**, 13147 (1999); K. Yang, S. Das Sarma, and A. H. MacDonald, Phys. Rev. B **74**, 075423 (2006).
- ²⁶ H.A. Fertig and L. Brey, Phys. Rev. Lett. **97**, 116805 (2006).
- ²⁷ G. Murthy, E. Shimshoni, and H. A. Fertig, Phys. Rev. B **90**, 241410 (2014).
- ²⁸ G. Murthy, E. Shimshoni, and H. A. Fertig, Phys. Rev. B **93**, 045105 (2016).
- ²⁹ P. Tikhonov, E. Shimshoni, H. A. Fertig, and G. Murthy, arXiv:1512.07825 (2015).
- ³⁰ A problem analogous to the edge of the F phase of the $\nu = 0$ state in graphene was earlier studied in V. I. Fal'ko and S. V. Iordanskii, Phys. Rev. Lett. **82**, 402 (1999), for QHFM's with the sign-changing Zeeman field.
- ³¹ T. Giamarchi, *Quantum Physics in One Dimension*, Oxford University Press (2003).
- ³² I.F. Herbut, Phys. Rev. B **76**, 085432 (2007).
- ³³ M. Kharitonov, Phys. Rev. B **85**, 155439 (2012).
- ³⁴ M. Kharitonov, Phys. Rev. Lett. **109**, 046803 (2012).
- ³⁵ M. Kharitonov, Phys. Rev. B **86**, 075450 (2012).
- ³⁶ D. I. Pikulin, P. G. Silvestrov, and T. Hyart, Nature Comm. **7**, 10462 (2016).
- ³⁷ S. L. Sondhi, A. Karlhede, S. A. Kivelson, and E. H. Rezayi, Phys. Rev. B **47**, 16419 (1993).
- ³⁸ P. Maher, C. R. Dean, A. F. Young, T. Taniguchi, K. Watanabe, K. L. Shepard, J. Hone, and P. Kim, Nature Physics **9**, 154 (2013).
- ³⁹ W. H. Press, S. A. Teukolsky, W. T. Vetterling, B. P. Flannery, *Numerical Recipes: The Art of Scientific Computing (3rd ed.)*, Cambridge University Press (2007).